
EXPLORING THE DESIGN SPACE OF DIFFUSION BRIDGE MODELS VIA STOCHASTICITY CONTROL

Shaorong Zhang

University of California Riverside
szhan311@ucr.edu

Yuanbin Cheng

University of California Riverside
ychen871@ucr.edu

Xianghao Kong

University of California Riverside
xkong016@ucr.edu

Greg Ver Steeg

University of California Riverside
greg.versteeg@ucr.edu

October 30, 2024

ABSTRACT

Diffusion bridge models effectively facilitate image-to-image (I2I) translation by connecting two distributions. However, existing methods overlook the impact of noise in sampling SDEs, transition kernel, and the base distribution on sampling efficiency, image quality and diversity. To address this gap, we propose the Stochasticity-controlled Diffusion Bridge (SDB), a novel theoretical framework that extends the design space of diffusion bridges, and provides strategies to mitigate singularities during both training and sampling. By controlling stochasticity in the sampling SDEs, our sampler achieves speeds up to $5\times$ faster than the baseline, while also producing lower FID scores. After training, SDB sets new benchmarks in image quality and sampling efficiency via managing stochasticity within the transition kernel. Furthermore, introducing stochasticity into the base distribution significantly improves image diversity, as quantified by a newly introduced metric.

1 Introduction

Denoising Diffusion Models (DDMs) create a stochastic process to transition Gaussian noise into a target distribution (Song & Ermon, 2019; Ho et al., 2020; Song et al., 2020). Building upon this, diffusion bridge-based models (DBMs) have been developed to transport between two arbitrary distributions, π_T and π_0 , including Bridge Matching (Peluchetti, 2023), Flow Matching (Lipman et al., 2022), and Stochastic Interpolants (Albergo et al., 2023). Compared to DDMs, DBMs offer greater versatility for tasks such as I2I translation (Linqi Zhou et al., 2023; Liu et al., 2023). This advantage arises because using a Gaussian prior often fails to incorporate sufficient knowledge about the target distribution.

In general, there are two primary design philosophies for DBMs. The first involves deriving a pinned process (Yifeng Shi et al., 2023) from a given reference process (e.g., Brownian motion) via Doob’s h -transform, and then constructing a bridge to approach it (Linqi Zhou et al., 2023; Peluchetti, 2023). The second regime aims to directly design a bridge based on a specified transition kernel (Lipman et al., 2022; Albergo et al., 2023). While the former also results in a transition kernel, the mean and variance in the kernel are *coupled*, which limits the design flexibility for possible bridges. In this work, we follow the second fashion and further propose the Stochasticity Control (SC) mechanism, which facilitates easier tuning and leads to enhanced performance across a variety of tasks. Our main contributions are as follows:

- We introduce the **Stochasticity-controlled Diffusion Bridge** (SDB), a generalized framework that adopts a transition kernel-based design philosophy to elucidate the design space of DBMs. Notably, this framework not only encompasses other mainstream DBMs such as DDBM (Linqi Zhou et al., 2023) and I2SB (Liu et al., 2023), but also DDMs like EDM (Karras et al., 2022), as detailed in Table 1.

- A **Stochasticity Control** (SC) mechanism is proposed by adding noise into the base distribution, designing a noise schedule for the transition kernel, and regulating the drift term in the sampling SDEs. In addition, we explore **score reparameterization** and the **discretization schemes** of sampling SDEs to mitigate singularity during training and sampling. These combined strategies lead to significant improvements in training stability, sampling efficiency, output quality, and conditional diversity.
- Experimental results show that our sampler operates $5\times$ faster than the DDBM sampler and achieves a lower FID score using the same pretrained models. When trained from scratch, our model sets a new benchmark for image quality, requiring only 5 function evaluations to reach an FID of 0.89. Furthermore, by introducing noise into the base distribution, we significantly enhance the diversity of synthetic images, resulting in a greater variety of colors and textures.

Notations Let π_T , π_0 , and π_{0T} represent the base distribution, the target distribution, and the joint distribution of them respectively. π_{cond} and π_{data} represent the distributions of the input and output data. Let p be the distribution of a diffusion process; we denote its marginal distribution at time t by p_t , the conditional distribution at time t given the state at time s by $p_{t|s}$, and the distribution at time t given the states at times 0 and T by $p_{t|0T}$, i.e., the transition kernel of a bridge.

2 Background

2.1 Denoising diffusion models

Denoising diffusion models map target distribution π_0 into a base distribution π_T by define a forward process on the time-interval $[0, T]$:

$$d\mathbf{X}_t = \bar{f}_t \mathbf{X}_t dt + \bar{g}_t d\mathbf{W}_t, \quad \mathbf{X}_0 \sim \pi_0, \quad (1)$$

where $\bar{f}_t, \bar{g}_t : [0, T] \rightarrow \mathbb{R}$ is the scalar-valued drift and diffusion term, $\mathbf{X}_0 \in \mathbb{R}^d$ is drawn from the target distribution π_0 , \mathbf{W}_t is a d -dimensional Wiener process. To sample from the target distribution π_0 , the generative model is given by the reverse SDE or ODE (Song et al., 2020):

$$d\mathbf{X}_t = [\bar{f}_t \mathbf{X}_t - \bar{g}_t^2 \nabla_{\mathbf{X}_t} \log q_t(\mathbf{X}_t)] dt + \bar{g}_t d\mathbf{W}_t, \quad \mathbf{X}_T \sim \pi_T, \quad (2)$$

$$d\mathbf{X}_t = \left[\bar{f}_t \mathbf{X}_t - \frac{1}{2} \bar{g}_t^2 \nabla_{\mathbf{X}_t} \log q_t(\mathbf{X}_t) \right] dt, \quad \mathbf{X}_T \sim \pi_T, \quad (3)$$

where q_t denotes the marginal distribution of this process. The score function $\nabla_{\mathbf{X}_t} \log q_t(\mathbf{X}_t)$ is approximated using a neural network $\mathbf{s}_\theta(\mathbf{x}_t, t)$, which can be learned by the score-matching loss:

$$\mathcal{L}(\theta) = \mathbb{E}_{\mathbf{x}_t \sim p_{t|0}(\mathbf{x}_t|\mathbf{x}_0), \mathbf{x}_0 \sim \pi_0, t \sim \mathcal{U}(0, T)} \left[\omega(t) \left\| \mathbf{s}_\theta(\mathbf{x}_t, t) - \nabla_{\mathbf{X}_t} \log q_{t|0}(\mathbf{x}_t|\mathbf{x}_0) \right\|^2 \right], \quad (4)$$

where $q_{t|0}$ is the analytic forward transition kernel and $\omega(t)$ is a positive weighting function.

2.2 Denoising Diffusion Bridge Models

DDBMs (Linqi Zhou et al., 2023) extend diffusion models to translate between two arbitrary distributions π_0 and π_T given samples from them. Consider a reference process in Eq. (1) with transition kernel $q_{t|0}(\mathbf{x}_t|\mathbf{x}_0) = \mathcal{N}(\mathbf{x}_t; a_t \mathbf{x}_0, \sigma_t^2 \mathbf{I})$, this process can be pinned down at an initial and terminal point $\mathbf{x}_0, \mathbf{x}_T$. Under mild assumptions, the pinned process is given by Doob's h -transform (Rogers & Williams, 2000):

$$d\mathbf{X}_t = \{\bar{f}_t \mathbf{X}_t + \bar{g}_t^2 \nabla_{\mathbf{X}_t} \log p_{T|t}(\mathbf{x}_T|\mathbf{X}_t)\} dt + \bar{g}_t d\mathbf{W}_t, \quad \mathbf{X}_0 = \mathbf{x}_0, \quad (5)$$

where $\nabla_{\mathbf{X}_t} \log p_{T|t}(\mathbf{x}_T \mid \mathbf{X}_t) = \frac{(a_t/a_T)\mathbf{x}_T - \mathbf{x}_t}{\sigma_t^2(\text{SNR}_t/\text{SNR}_{T-1})}$ and $\text{SNR} := a_t^2/\sigma_t^2$ (Linqi Zhou et al., 2023). The marginal density of process (5) serves as transition kernel and is given by $p(\mathbf{x}_t|\mathbf{x}_0, \mathbf{x}_T) = \mathcal{N}(\mathbf{x}_t; \alpha_t \mathbf{x}_0 + \beta_t \mathbf{x}_T, \gamma_t^2 \mathbf{I})$, where $\alpha_t = a_t(1 - \frac{\text{SNR}_T}{\text{SNR}_t})$, $\beta_t = \frac{a_t}{a_T} \frac{\text{SNR}_T}{\text{SNR}_t}$, $\gamma_t^2 = \sigma_t^2(1 - \frac{\text{SNR}_T}{\text{SNR}_t})$.

To sample from the conditional distribution $p(\mathbf{x}_0|\mathbf{x}_T)$, we can solve the reverse SDE or probability flow ODE from $t = T$ to $t = 0$:

$$d\mathbf{X}_t = \{\bar{f}_t \mathbf{X}_t + \bar{g}_t^2 (\nabla_{\mathbf{X}_t} \log p_{T|t}(\mathbf{x}_T|\mathbf{X}_t) - \nabla_{\mathbf{X}_t} \log p_{t|T}(\mathbf{X}_t|\mathbf{x}_T))\} dt + \bar{g}_t d\mathbf{W}_t, \mathbf{X}_T = \mathbf{x}_T \quad (6)$$

$$d\mathbf{X}_t = \{\bar{f}_t \mathbf{X}_t + \bar{g}_t^2 (\nabla_{\mathbf{X}_t} \log p_{T|t}(\mathbf{x}_T|\mathbf{X}_t) - \frac{1}{2} \nabla_{\mathbf{X}_t} \log p_{t|T}(\mathbf{X}_t|\mathbf{x}_T))\} dt, \quad \mathbf{X}_T = \mathbf{x}_T. \quad (7)$$

Generally, the score $\nabla_{\mathbf{x}_t} \log p_{t|T}(\mathbf{x}_t|\mathbf{x}_T)$ in Eqs. (6) and (7) is intractable. However, it can be effectively estimated by denoising bridge score matching. Let $(\mathbf{x}_0, \mathbf{x}_T) \sim \pi_{0,T}(\mathbf{x}_0, \mathbf{x}_T)$, $\mathbf{x}_t \sim p_{t|0,T}(\mathbf{x}_t|\mathbf{x}_0, \mathbf{x}_T)$, $t \sim \mathcal{U}(0, T)$, and $\omega(t)$ be non-zero loss weighting term of any choice, then the score $\nabla_{\mathbf{x}_t} \log p_{T|t}(\mathbf{x}_T|\mathbf{x}_t)$ can be approximated by a neural network $\mathbf{s}_\theta(\mathbf{x}_t, \mathbf{x}_T, t)$ with denoising bridge score matching objective:

$$\mathcal{L}(\theta) = \mathbb{E}_{\mathbf{x}_t, \mathbf{x}_0, \mathbf{x}_T, t} [w(t) \|\mathbf{s}_\theta(\mathbf{X}_t, \mathbf{x}_T, t) - \nabla_{\mathbf{x}_t} \log p_{t|0,T}(\mathbf{X}_t | \mathbf{x}_0, \mathbf{x}_T)\|^2]. \quad (8)$$

To sum up, DDBM starts with the forward SDE outlined in Eq. (1) with a marginal distribution of $q_{t|0}(\mathbf{x}_t|\mathbf{x}_0) = \mathcal{N}(\mathbf{x}_t; a_t \mathbf{x}_0, \sigma_t^2 \mathbf{I})$. The pinned process is then built by applying Doob's h -transform as specified in Eq. (5), which is unnecessarily complicated and constraining. Additionally, the transition kernel of the pinned process becomes complex and coupled, as α_t , β_t , and γ_t are all interrelated through a_t and σ_t , increasing the design difficulty. In the next section, we will demonstrate how α_t and β_t can be used to control interpolation, while γ_t is designed to regulate the stochasticity introduced into the path.

3 Stochasticity control

3.1 Stochasticity control in transition kernel

We are interested in building a diffusion process to transport from two arbitrary distributions π_T and π_0 . Suppose the transition kernel of this process is $p_{t|0,T}(\mathbf{x}_t|\mathbf{x}_0, \mathbf{x}_T) = \mathcal{N}(\mathbf{x}_t; \alpha_t \mathbf{x}_T + \beta_t \mathbf{x}_0, \gamma_t^2 \mathbf{I})$. To ensure that the process originates from \mathbf{x}_0 and concludes at \mathbf{x}_T , we set $\alpha_0 = \beta_T = 1$ and $\alpha_T = \beta_0 = 0$. Additionally, we require $\alpha_t, \beta_t, \gamma_t > 0$ for $t \in (0, T)$.

Let $T = 1$, one simple design example involves defining α_t and β_t linearly, such that $\alpha_t = 1 - t$ and $\beta_t = t$, with $\gamma_t = 2\gamma_{\max} \sqrt{t(1-t)}$, where γ_{\max} is a constant representing the maximum noise level. This configuration is referred to as the *linear* path for transition kernel. Other designs such as $\alpha_t = \cos(\pi t/2)$, $\beta_t = \sin(\pi t/2)$, and $\gamma_t = \sin(\pi t)$ can also be employed. Notably, the DDBM-VP and DDBM-VE models presented in (Linqi Zhou et al., 2023) can be considered as special cases within our framework, contingent upon the specific choices of α_t , β_t , and γ_t . We illustrate some design choices of different paths in Fig. 1.

There are infinitely many pinned processes characterized by the Gaussian transition kernel $p_{t|0,T}(\mathbf{x}_t | \mathbf{x}_0, \mathbf{x}_T) = \mathcal{N}(\mathbf{x}_t; \alpha_t \mathbf{x}_0 + \beta_t \mathbf{x}_T, \gamma_t^2 \mathbf{I})$. Specifically, we formalize the pinned process as a linear Itô SDE, as presented in Lemma 1.

Lemma 1. *There exist a linear Itô SDE*

$$d\mathbf{X}_t = [f_t \mathbf{X}_t + s_t \mathbf{x}_T] dt + g_t d\mathbf{W}_t, \quad \mathbf{X}_0 = \mathbf{x}_0, \quad (9)$$

where $f_t = \frac{\dot{\alpha}_t}{\alpha_t}$, $s_t = \dot{\beta}_t - \frac{\dot{\alpha}_t}{\alpha_t} \beta_t$, $g_t = \sqrt{2(\gamma_t \dot{\gamma}_t - \frac{\dot{\alpha}_t}{\alpha_t} \gamma_t^2)}$, that has a Gaussian marginal distribution $\mathcal{N}(\mathbf{x}_t; \alpha_t \mathbf{x}_0 + \beta_t \mathbf{x}_T, \gamma_t^2 \mathbf{I})$.

Given the pinned process (9), we can sample from the conditional distribution $p_{0|T}(\mathbf{x}_0|\mathbf{x}_T)$ by solving the reverse SDE or ODE from $t = T$ to $t = 0$:

$$d\mathbf{X}_t = [f_t \mathbf{X}_t + s_t \mathbf{x}_T - g_t^2 \nabla_{\mathbf{X}_t} \log p_t(\mathbf{X}_t|\mathbf{x}_T)] dt + g_t d\mathbf{W}_t, \quad \mathbf{X}_T = \mathbf{x}_T, \quad (10)$$

$$d\mathbf{X}_t = \left[f_t \mathbf{X}_t + s_t \mathbf{x}_T - \frac{1}{2} g_t^2 \nabla_{\mathbf{X}_t} \log p_t(\mathbf{X}_t|\mathbf{x}_T) \right] dt, \quad \mathbf{X}_T = \mathbf{x}_T, \quad (11)$$

where the score $\nabla_{\mathbf{X}_t} \log p_t(\mathbf{X}_t|\mathbf{x}_T)$ can be estimated by score matching objective (8). To improve training stability, we introduced score reparameterization in Sec. 4.1.

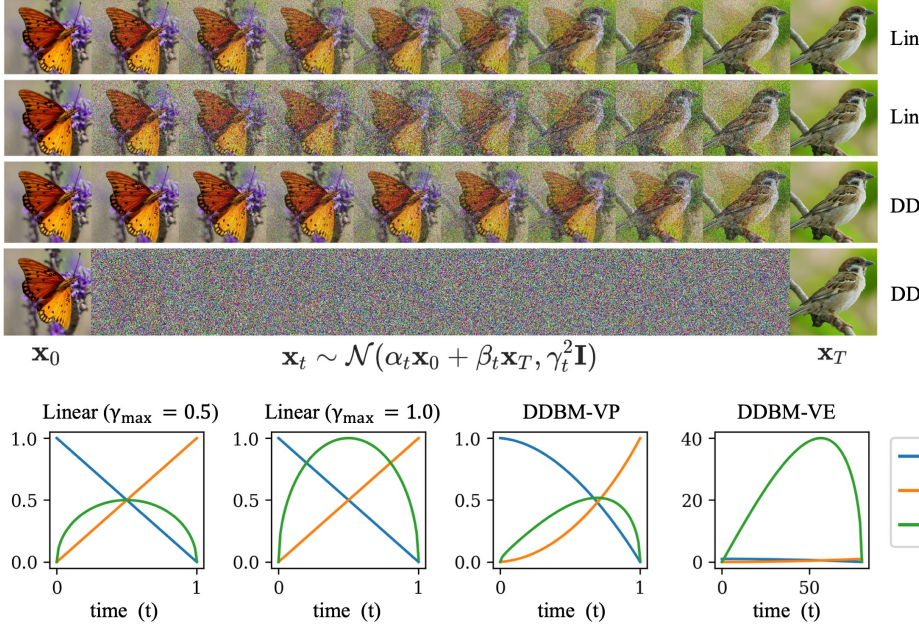


Figure 1: An illustration of design choices of transition kernels and how they affect the I2I translation process. α_t and β_t define the interpolation between two images, while γ_t controls the noise added to the process.

3.2 Stochasticity control in sampling SDEs

Stochasticity control (SC) during the sampling phase has been explored for diffusion models by Karras et al. (2022), yet comprehensive studies on its application to diffusion bridge models remain limited. Eqs. (10) and (11) offer sampling schemes that align with Eqs. (6) and (7) in the DDBM framework. However, these methods do not guarantee optimal performance in terms of sampling speed and image quality. To address this issue, Linqi Zhou et al. (2023) introduced a hybrid sampler alternating between reversed ODE and SDE, and Zheng et al. (2024) accelerated sampling with an improved algorithm using discretized timesteps. This section aims to explore how SC can be further optimized in the sampling for DBMs, thereby addressing the current research gap.

For dynamics described by ODE $d\mathbf{X}_t = \mathbf{u}_t dt$, we can identify the entire class of SDEs that maintain the same marginal distributions, as detailed in Lemma 2. This enables us to control the stochasticity during sampling by appropriately designing ϵ_t .

Lemma 2. Consider a continuous dynamics given by ODE of the form: $d\mathbf{X}_t = \mathbf{u}_t dt$, with the density evolution $p_t(\mathbf{X}_t)$. Then there exists forward SDEs and backward SDEs that match the marginal distribution p_t . The forward SDEs are given by: $d\mathbf{X}_t = (\mathbf{u}_t + \epsilon_t \nabla \log p_t) dt + \sqrt{2\epsilon_t} d\mathbf{W}_t$, $\epsilon_t > 0$. The backward SDEs are given by: $d\mathbf{X}_t = (\mathbf{u}_t - \epsilon_t \nabla \log p_t) dt + \sqrt{2\epsilon_t} d\mathbf{W}_t$, $\epsilon_t > 0$.

Lemma 2 is readily implementable, requiring only the specification of an ODE. Here ϵ_t controls the stochasticity added to the process at time t . For diffusion bridge models, the ODE formulation is presented in Eq. (11), which underpins the SC strategy in Theorem 3.

Theorem 3. Suppose the transition kernel of a diffusion process is given by $p_{t|0,T}(\mathbf{x}_t \mid \mathbf{x}_0, \mathbf{x}_T) = \mathcal{N}(\mathbf{x}_t; \alpha_t \mathbf{x}_0 + \beta_t \mathbf{x}_T, \gamma_t^2 \mathbf{I})$, then the evolution of conditional probability $q(\mathbf{X}_t \mid \mathbf{x}_T)$ has a class of time reverse sampling SDEs of the form:

$$d\mathbf{X}_t = \left[\dot{\alpha}_t \hat{\mathbf{x}}_0 + \dot{\beta}_t \mathbf{x}_T - (\dot{\gamma}_t \gamma_t + \epsilon_t) \nabla_{\mathbf{X}_t} \log p_t(\mathbf{X}_t \mid \mathbf{x}_T) \right] dt + \sqrt{2\epsilon_t} d\mathbf{W}_t \quad \mathbf{X}_T = \mathbf{x}_T. \quad (12)$$

Remark 3.1. As $\epsilon_t = 0$, Eq. (12) recovers the sampling ODE specified in Eq. (11). As $\epsilon_t = \gamma_t \dot{\gamma}_t - \frac{\dot{\alpha}_t}{\alpha_t} \gamma_t^2$, Eq. (12) recovers the sampling ODE specified in Eq. (10). As $\epsilon_t = \eta(\gamma_t \dot{\gamma}_t - \frac{\dot{\alpha}_t}{\alpha_t} \gamma_t^2)$, $\eta \in (0, 1)$, the stochasticity is between the original sampling ODE in Eq. (11) and SDE in Eq. (10).

Table 1: Specify design choices for different model families. In the implementation, $\sigma_t = t$ for EDM, $\sigma_t = t, a_t = 1$ for DDBM-VE, $\sigma_t = \sqrt{e^{\frac{1}{2}\beta_d t^2 + \beta_{\min} t} - 1}$ and $a_t = 1/\sqrt{e^{\frac{1}{2}\beta_d t^2 + \beta_{\min} t}}$ for DDBM-VP, where β_d and β_{\min} are parameters. We include details and proofs in Appendix B.

		I2SB	DDBM	EDM	Ours
SC-transition kernel Sec. 3.1	α_t	$1 - \sigma_t^2/\sigma_T^2$	$a_t(1 - a_T^2\sigma_t^2/(\sigma_t^2 a_t^2))$	1	$1 - t$
	β_t	σ_t^2/σ_T^2	$a_T\sigma_t^2/(\sigma_t^2 a_t)$	0	t
	γ_t^2	$\sigma_t^2(1 - \sigma_t^2/\sigma_T^2)$	$\sigma_t^2(1 - a_T^2\sigma_t^2/(\sigma_t^2 a_t^2))$	σ_t^2	$\frac{\gamma_{\max}^2}{4}t(1 - t)$
SC-sampling SDEs Sec. 3.2	ϵ_t	$\frac{\gamma_t^2 - \Delta t \beta_t^2 - \beta_{t-\Delta t}^2 \gamma_t^2}{2\beta_t^2 \Delta t}$	$\eta(\gamma_t \dot{\gamma}_t - \frac{\dot{\alpha}_t}{\alpha_t} \gamma_t^2)$ $\eta = 0 \text{ or } \eta = 1$	$\bar{\beta}_t \sigma_t^2$ -	$\eta(\gamma_t \dot{\gamma}_t - \frac{\dot{\alpha}_t}{\alpha_t} \gamma_t^2)$ $\eta \in [0, 1]$
	SC-base distribution Sec. 3.3	π_T	π_{cond}	π_{cond}	$\pi_{\text{cond}} * \mathcal{N}(0, b^2 \mathbf{I})$
Score reparameterization Sec. 4.1	s_θ	$\frac{\alpha_t \hat{\mathbf{x}}_0 + \beta_t \mathbf{x}_T - \mathbf{x}_t}{\gamma_t^2}$	$\frac{\alpha_t \hat{\mathbf{x}}_0 + \beta_t \mathbf{x}_T - \mathbf{x}_t}{\gamma_t^2}$	$\frac{\alpha_t \hat{\mathbf{x}}_0 + \beta_t \mathbf{x}_T - \mathbf{x}_t}{\gamma_t^2}$	$\frac{\alpha_t \hat{\mathbf{x}}_0 + \beta_t \mathbf{x}_T - \mathbf{x}_t}{\gamma_t^2}$
Discretization Sec. 4.2	-	Euler Eq. (20)	Euler Eq. (17)	Heun -	Euler Eqs. (17) and (19)

There is no definitive principle for designing ϵ_t . For DDMs, Karras et al. (2022) suggest that the optimal level of stochasticity should be determined empirically. In the case of DBMs, however, certain design guidelines can be followed to potentially enhance performance. Unlike DDMs, which typically start sampling from Gaussian noise, DBMs begin with a deterministic condition \mathbf{x}_T . Therefore, setting $\epsilon_t = 0$ results in no stochasticity for the sampling process and final sample \mathbf{x}_0 , which may partly explain the poor performance of ODE samplers in this context. However, it is advantageous to set $\epsilon_t = 0$ during the final steps of sampling. The rationale behind this approach is discussed in detail in Section 4.2.

3.3 Stochasticity control in base distribution

Conditional diversity refers to the range of outputs that can be generated from specific conditions. This is valuable in scenarios like image generation from edges, where one edge image may lead to multiple valid images differing in color, texture, or detail. Conversely, in super-resolution, where a high-resolution image is created from a low-resolution one, output variability is limited by the input's structure, demanding consistency and fidelity to the original rather than diversity.

To control the conditional diversity of diffusion bridge models, we can trade off between DBMs and DDMs by controlling the stochasticity in the base distribution. Bridge models transport the base distribution π_T to target distribution π_0 . Typically, most previous bridge models, such as those discussed in (Linqi Zhou et al., 2023; Albergo et al., 2023), treat π_T as the input data distribution, π_{cond} . However, it is flexible to design π_T ; for instance, by choosing π_T as a Gaussian distribution, we recover DDMs. An intermediate approach involves the convolution of π_{cond} with a Gaussian distribution, $\pi_T = \pi_{\text{cond}} * \mathcal{N}(0, b^2 \mathbf{I})$, where b is a constant that controls the strength of booting noise we added to the input data distribution. We provide an illustration of the effect of SC in transition kernel, sampling SDEs and distribution in Fig. 2.

We developed the Average Feature Distance (AFD) metric to quantify the conditional diversity among generated images. Initially, we select a group of source images $\{\mathbf{x}_T^{(i)}\}_{i=1}^M$. For each $\mathbf{x}_T^{(i)}$, we then generate L distinct target samples. The j -th generated sample corresponding to the i -th source image is denoted by \mathbf{y}_{ij} . Then the AFD is calculated as follows:

$$\text{AFD} = \frac{1}{M} \sum_{i=1}^M \frac{1}{L^2 - L} \sum_{k,l=1, k \neq l}^L \|F(\mathbf{y}_{ik}) - F(\mathbf{y}_{il})\| \quad (13)$$

where $F(\cdot)$ is a function that extracts the features of images, and $\|\cdot\|$ represents Euclidean norm. Intuitively, a larger AFD indicates the better conditional diversity. Here, $F(\mathbf{x})$ can be \mathbf{x} to evaluate the diversity directly in the pixel

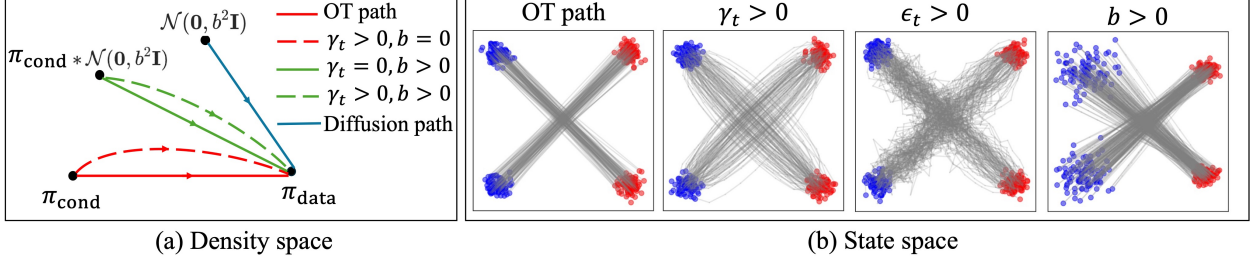


Figure 2: The effect of stochasticity control on density and state spaces. Adding no stochasticity ($\gamma_t = 0, \epsilon_t = 0, b = 0$) leads to the optimal transport (OT) path. (a). In the density space, OT path directly links π_{cond} and π_{data} , while diffusion path transports from $\mathcal{N}(0, b^2 \mathbf{I})$ to π_{data} . When $\gamma_t > 0$ (dash lines), it increases stochasticity in the middle of the transition, whereas $b > 0$ (green lines), it directly adds stochasticity to the base distribution, leading to trade off between DDMs and DBMs when $b = 0$. (b). In the state space, we use blue dots and red dots to represent input and output data respectively. The OT path directly links two samples, it shows a detoured path when $\gamma_t > 0$, introduces a zigzag pattern while $\epsilon_t > 0$, and smooths the base distribution as $b > 0$.

space. Alternatively, $F(\cdot)$ can be defined using the Inception-V3 model to assess the diversity in the latent space. In our experiments, we use AFD in latent space.

4 Score reparameterization and Algorithm design

4.1 Score reparameterization

The log gradient of Gaussian transition kernel $p_{t|0,T}(\mathbf{x}_t | \mathbf{x}_0, \mathbf{x}_T) = \mathcal{N}(\mathbf{x}_t; \alpha_t \mathbf{x}_0 + \beta_t \mathbf{x}_T, \gamma_t^2 \mathbf{I})$ has an analytical form: $\nabla_{\mathbf{x}_t} \log p_{t|0,T}(\mathbf{x}_t | \mathbf{x}_0, \mathbf{x}_T) = (\alpha_t \mathbf{x}_0 + \beta_t \mathbf{x}_T - \mathbf{x}_t) / \gamma_t^2$. Therefore, the denoising bridge score matching objective in Eq. (8) is tractable. However, the singular term $1/\gamma_t^2$ at endpoints $t = 0$ and $t = T$ can lead to highly unstable training. Consequently, instead of directly parameterizing the score function $\nabla_{\mathbf{x}_t} \log p_t(\mathbf{x}_t | \mathbf{x}_T)$ with a neural network, we opt to reparameterize the score as a function of $\hat{\mathbf{x}}_0(\mathbf{x}_t, \mathbf{x}_T, t)$, as demonstrated in Theorem 4. This reparameterization strategy, initially introduced in EDM (Karras et al., 2022), is particularly significant for enhancing the stability and performance of our bridge models.

Theorem 4. *Let $(\mathbf{x}_0, \mathbf{x}_T) \sim \pi_0(\mathbf{x}_0, \mathbf{x}_T)$, $\mathbf{x}_t \sim p_{t|0,T}(\mathbf{x}_t | \mathbf{x}_0, \mathbf{x}_T)$, $t \sim \mathcal{U}(0, T)$. Given the transition kernel: $p_{t|0,T}(\mathbf{x}_t | \mathbf{x}_0, \mathbf{x}_T) = \mathcal{N}(\mathbf{x}_t; \alpha_t \mathbf{x}_0 + \beta_t \mathbf{x}_T, \gamma_t^2 \mathbf{I})$, if $\hat{\mathbf{x}}_0(\mathbf{x}_t, \mathbf{x}_T, t)$ is a denoiser function that minimizes the expected L_2 denoising error for samples drawn from $\pi_0(\mathbf{x}_0, \mathbf{x}_T)$:*

$$\hat{\mathbf{x}}_0(\mathbf{x}_t, \mathbf{x}_T, t) = \arg \min_{D(\mathbf{x}_t, \mathbf{x}_T, t)} \mathbb{E}_{\mathbf{x}_0, \mathbf{x}_T, \mathbf{x}_t} [\lambda(t) \|D(\mathbf{x}_t, \mathbf{x}_T, t) - \mathbf{x}_0\|_2^2], \quad (14)$$

then the score has the following relationship with $\hat{\mathbf{x}}_0(\mathbf{x}_t, \mathbf{x}_T, t)$:

$$\nabla_{\mathbf{x}_t} \log p_t(\mathbf{x} | \mathbf{x}_T) = \frac{\alpha_t \hat{\mathbf{x}}_0(\mathbf{x}, \mathbf{x}_T, t) + \beta_t \mathbf{x}_T - \mathbf{x}_t}{\gamma_t^2}. \quad (15)$$

The key observation is that $\hat{\mathbf{x}}_0(\mathbf{x}_t, \mathbf{x}_T, t)$ can be estimated by a neural network $D_\theta(\mathbf{x}_t, \mathbf{x}_T, t)$ trained according to Eq. (14). In the implementation, we include additional pre- and post-processing steps: scaling functions and loss weighting, see Appendix C for details.

4.2 Algorithm design

Let $\hat{\mathbf{z}}_t =: (\mathbf{x}_t - \alpha_t \hat{\mathbf{x}}_0 - \beta_t \mathbf{x}_T) / \gamma_t$, then the score $\nabla_{\mathbf{x}_t} \log p_t(\mathbf{x} | \mathbf{x}_T)$ and $\hat{\mathbf{z}}_t$ has a linear relationship: $\hat{\mathbf{z}}_t = -\gamma_t \nabla_{\mathbf{x}_t} \log p_t(\mathbf{x} | \mathbf{x}_T)$. An alternative formulation of the sampling SDEs (12) is presented as:

$$d\mathbf{X}_t = \left[\dot{\alpha}_t \hat{\mathbf{x}}_0 + \dot{\beta}_t \mathbf{x}_T + (\dot{\gamma}_t + \frac{\epsilon_t}{\gamma_t}) \hat{\mathbf{z}}_t \right] dt + \sqrt{2\epsilon_t} d\mathbf{W}_t. \quad (16)$$

Instead of using the score directly, we apply Eq. (16) to reduce truncation error. Additionally, $\hat{\mathbf{z}}$ can be seen as the estimated noise added to the interpolation (Albergo et al., 2023), the introduction of $\hat{\mathbf{z}}$ brings more interpretability. One discretization scheme of sampling SDEs Eq. (16) is based on Euler's method:

$$\mathbf{x}_{t-\Delta t} \approx \mathbf{x}_t - \left[\dot{\alpha}_t \hat{\mathbf{x}}_0 + \dot{\beta}_t \mathbf{x}_T + \left(\dot{\gamma}_t + \frac{\epsilon_t}{\gamma_t} \right) \hat{\mathbf{z}} \right] \Delta t + \sqrt{2\epsilon_t \Delta t} \bar{\mathbf{z}}_t, \quad \bar{\mathbf{z}}_t \sim \mathcal{N}(0, \mathbf{I}). \quad (17)$$

Furthermore, for small enough Δt the derivative term can be approximated by: $\dot{\alpha}_t \approx (\alpha_t - \alpha_{t-\Delta t})/\Delta t$, $\dot{\beta}_t \approx (\beta_t - \beta_{t-\Delta t})/\Delta t$, $\dot{\gamma}_t \approx (\gamma_t - \gamma_{t-\Delta t})/\Delta t$. Using the fact that $\mathbf{x}_t = \alpha_t \hat{\mathbf{x}}_0 + \beta_t \mathbf{x}_T + \gamma_t \hat{\mathbf{z}}_t$, we can further simplify the iteration:

$$\mathbf{x}_{t-\Delta t} \approx \alpha_{t-\Delta t} \hat{\mathbf{x}}_0 + \beta_{t-\Delta t} \mathbf{x}_T + \left(\gamma_{t-\Delta t} - \frac{\epsilon_t \Delta t}{\gamma_t} \right) \hat{\mathbf{z}}_t + \sqrt{2\epsilon_t \Delta t} \bar{\mathbf{z}}_t. \quad (18)$$

As $\gamma_{t-\Delta t}^2 - 2\epsilon_t \Delta t > 0$, $\gamma_{t-\Delta t} - \frac{\epsilon_t \Delta t}{\gamma_t} \approx \sqrt{\gamma_{t-\Delta t}^2 - 2\epsilon_t \Delta t}$, which leads to another discretization and recovers the sampler of DBIM (Zheng et al., 2024):

$$\mathbf{x}_{t-\Delta t} = \alpha_{t-\Delta t} \hat{\mathbf{x}}_0 + \beta_{t-\Delta t} \mathbf{x}_T + \sqrt{\gamma_{t-\Delta t}^2 - 2\epsilon_t \Delta t} \hat{\mathbf{z}}_t + \sqrt{2\epsilon_t \Delta t} \bar{\mathbf{z}}_t. \quad (19)$$

Remark 4.1. Eq. (19) provides more insight about the noise and the design of ϵ_t . Here $\hat{\mathbf{z}}_t$ and $\bar{\mathbf{z}}_t$ serve as predicted noise and added noise respectively. Generally, we assume the error $\|\mathbf{x}_0 - \hat{\mathbf{x}}_0(\mathbf{x}_t, \mathbf{x}_T, t)\|$ decreases as we move \mathbf{x}_t from \mathbf{x}_T to \mathbf{x}_0 . Therefore, a small ϵ_t was suggested as t close to 0. Further, due to the singular term $\epsilon_t \Delta t / \gamma_t$ at $t = 0$, it's better to set ϵ_t small enough to avoid singularity.

Remark 4.2. Eq. (19) requires a constraint $\gamma_{t-\Delta t}^2 - 2\epsilon_t \Delta t > 0$. Note that this limitation is unnecessary and will limit the design of ϵ_t .

As $2\epsilon_t \Delta t = \gamma_{t-\Delta t}^2 - \beta_{t-\Delta t}^2 \gamma_t^2 / \beta_t^2$, the coefficient of \mathbf{x}_t in Eq. 19 is 0, thus Eq. 19 can be simplified as:

$$\mathbf{x}_{t-\Delta t} = \left(\alpha_{t-\Delta t} - \alpha_t \frac{\beta_{t-\Delta t}}{\beta_t} \right) \hat{\mathbf{x}}_0 + \frac{\beta_{t-\Delta t}}{\beta_t} \mathbf{x}_t + \sqrt{\gamma_{t-\Delta t}^2 - \frac{\beta_{t-\Delta t}^2 \gamma_t^2}{\beta_t^2}} \bar{\mathbf{z}}_t \quad (20)$$

Remark 4.3. Eq. 20 is referred as Markovian bridge in Zheng et al. (2024), and this setting can be used to reproduce the sampler in I2SB Liu et al. (2023), see Appendix B for more details.

In our implementation, when we make $\epsilon_t = 0$ for the last two steps, Eq. (19) gets reduced to: $\mathbf{x}_{t-\Delta t} \approx \alpha_{t-\Delta t} \hat{\mathbf{x}}_0 + \beta_{t-\Delta t} \mathbf{x}_T + \gamma_{t-\Delta t} \hat{\mathbf{z}}_t$. For other steps, we apply Eq. (17) and let $\epsilon_t = \eta(\gamma_t \dot{\gamma}_t - \frac{\dot{\alpha}_t}{\alpha_t} \gamma_t^2)$, where η is a constant. Putting all ingredients together leads to our sampler outlined in Algorithm 1.

Algorithm 1 Denoising Diffusion Bridge Stochastic Sampler

Require: model $D_\theta(\mathbf{x}_t, \mathbf{x}_T, t)$, time steps $\{t_j\}_{j=0}^N$, input data distribution π_{cond} , scheduler $\alpha_t, \beta_t, \gamma_t, \epsilon_t, b$.

- 1: Sample $\mathbf{x}_T \sim \pi_{\text{cond}}$, $\mathbf{n}_0 \sim \mathcal{N}(0, b^2 \mathbf{I})$
- 2: $\mathbf{x}_N = \mathbf{x}_T + \mathbf{n}_0$
- 3: **for** $i = N, \dots, 1$ **do**
- 4: $\hat{\mathbf{x}}_0 \leftarrow D_\theta(\mathbf{x}_i, \mathbf{x}_T, t_i)$
- 5: $\hat{\mathbf{z}}_i \leftarrow (\mathbf{x}_i - \alpha_{t_i} \hat{\mathbf{x}}_0 - \beta_{t_i} \mathbf{x}_N) / \gamma_{t_i}$
- 6: **if** $N \geq 2$ **then**
- 7: Sample $\bar{\mathbf{z}}_i \sim \mathcal{N}(0, \mathbf{I})$
- 8: $d_i \leftarrow \dot{\alpha}_{t_i} \hat{\mathbf{x}}_0 + \dot{\beta}_{t_i} \mathbf{x}_N + (\dot{\gamma}_{t_i} + \epsilon_{t_i} / \gamma_{t_i}) \hat{\mathbf{z}}_i$
- 9: $\mathbf{x}_{i-1} \leftarrow \mathbf{x}_i + d_i(t_i - t_{i-1}) + \sqrt{2\epsilon_{t_i}(t_i - t_{i-1})} \bar{\mathbf{z}}_i$
- 10: **else**
- 11: $\mathbf{x}_{i-1} \leftarrow \alpha_{t_{i-1}} \hat{\mathbf{x}}_0 + \beta_{t_{i-1}} \hat{\mathbf{x}}_N + \gamma_{t_{i-1}} \hat{\mathbf{z}}_i$
- 12: **end if**
- 13: **end for**

Table 2: Ablation Study of ϵ_t via DDBM pretrained VP model (Evaluated by FID). $\epsilon_t = 0$ for the last 2 steps, otherwise $\epsilon_t = \eta(\gamma_t \dot{\gamma}_t - \frac{\dot{\alpha}_t}{\alpha_t} \gamma_t^2)$.

Sampler	η	NFE					
		5			10		
		Edges→Handbags (64 × 64)			DIODE-Outdoor (256 × 256)		
DDBM (Linqi Zhou et al., 2023)	-	317.22	137.15	46.74	328.33	151.93	41.03
DBIM (Zheng et al., 2024)	-	3.60	2.46	1.74	14.25	7.98	4.99
SDB (Ours)	0	10.89	11.45	11.69	77.31	84.68	87.34
	0.3	2.36	2.25	1.53	10.87	6.83	4.12
	0.5	10.21	7.17	4.18	18.94	12.91	8.07
	0.8	16.33	14.29	9.33	25.90	18.25	11.74
	1.0	18.78	17.61	13.59	30.62	21.64	14.08

Table 3: Quantitative results in the I2I translation task edges2handbags. Our results were achieved by Linear transition kernel and setting $\gamma_{\max} = 0.125$ and $\eta = 1$.

Model	NFE	FID ↓	IS ↑	LPIPS ↓	MSE
Pix2Pix (Isola et al., 2017)	1	74.8	3.24	0.356	0.209
DDIB (Su et al., 2022)	$\geq 40^{\dagger}$	186.84	2.04	0.869	1.05
SDEdit (Meng et al., 2021)	≥ 40	26.5	3.58	0.271	0.510
Rectified Flow (Liu et al., 2022b)	≥ 40	25.3	2.80	0.241	0.088
I ² SB (Liu et al., 2023)	≥ 40	7.43	3.40	0.244	0.191
DDBM (Linqi Zhou et al., 2023)	118	1.83	3.73	0.142	0.040
DDBM (Linqi Zhou et al., 2023)	200	0.88	3.69	0.110	0.006
DBIM (Zheng et al., 2024)	20	1.74	3.64	0.095	0.005
DBIM (Zheng et al., 2024)	100	0.89	3.62	0.100	0.006
SDB (Ours)	5	0.89	4.10	0.049	0.024
	10	0.67	4.11	0.045	0.024
	20	0.56	4.11	0.044	0.024

5 Experiments

In this section, we demonstrate that SDBs achieve much better performance for I2I transition tasks, in terms of sample efficiency, image quality and conditional diversity. We evaluate on I2I translation tasks on Edges→Handbags (Isola et al., 2017) scaled to 64×64 pixels and DIODE-Outdoor scaled to 256×256 (Vasiljevic et al., 2019). For evaluation metrics, we use Fréchet Inception Distance (FID) (Heusel et al., 2017) for all experiments, and additionally measure Inception Scores (IS) (Barratt & Sharma, 2018), Learned Perceptual Image Patch Similarity (LPIPS) (Zhang et al., 2018), Mean Square Error (MSE), following previous works (Zheng et al., 2024; Linqi Zhou et al., 2023). In addition, we use AFD, Eq. 13, to measure conditional diversity. Further details of the experiments are provided in Appendix C.

Stochasticity control in sampling SDEs. By specifically designing stochasticity control during sampling, our sampler surpasses the sampling results by DDBM and DBIM with the same pretrained model. The results are demonstrated in Table 2. We set the number of function evaluations (NFEs) from the set [5, 10, 20] and select η from the set [0, 0.3, 0.5, 0.8, 1.0]. We observed that our sampler achieves much lower FID compared to both DDBM sampler and DBIM sampler across all datasets and NFEs. Besides, the best performance achieved around $\eta = 0.3$, which is align with the total stochasticity added to the sampling process by original DDBM sampler (Linqi Zhou et al., 2023). The above results demonstrate the significance of designing the stochasticity added to the sampling process.

Stochasticity control in transition kernel. Despite the extensive design space available for the transition kernel, this paper focuses on linear transition path with different strength of maximum stochasticity, i.e., $p_{t|0,T}(\mathbf{x}_t|\mathbf{x}_0, \mathbf{x}_T) = \mathcal{N}(\mathbf{x}_t; (1-t)\mathbf{x}_0 + t\mathbf{x}_T, \frac{1}{4}\gamma_{\max}^2 t(1-t)\mathbf{I})$. Specifically, $\gamma_{\max} \in [0.125, 0.5, 1.0]$. We achieve optimal results with $\gamma_{\max} = 0.125$ (see Table 3). Our models establish a new benchmark for image quality, as evaluated by FID, IS and LPIPS. Despite our models having slightly higher MSEs compared to the baseline DDBM and DBIM, we believe that a larger MSE indicates that the generated images are distinct from their references, suggesting a richer diversity. We also provide the visualization of sampling process in Fig. 3.

Stochasticity control in base distribution. Through controlling stochasticity in the base distribution, we achieved a more diverse set of sample images, while this diversity comes at the cost of slightly higher FID scores and slower sampling speed. We show generated images in Fig. 4. More visualization can be found in Appendix D, which shows

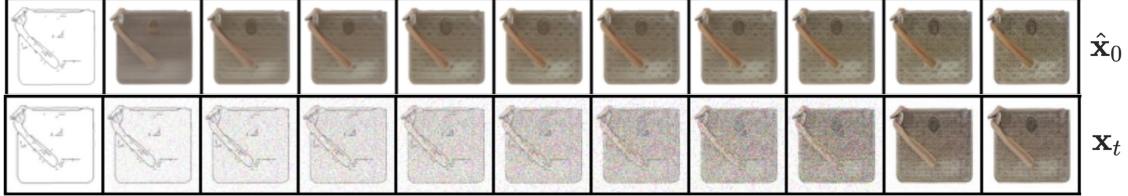


Figure 3: Visualization of the sampling process. The trajectories of \hat{x}_0 suggest that in the initial stage of the diffusion model, more general features such as shape and color are constructed. As the process evolves, it progressively generates finer details and high-frequency elements like texture.



Figure 4: Visualization of conditional diversity via sampled images. Compared with DDBM-VP, Our model demonstrates the ability to generate images with more colors and patterns given certain edges.

Table 4: Quantitative results for sample efficiency, image quality, and conditional diversity. By adding stochasticity to the base distribution ($b > 0$), we achieved much better conditional diversity, evaluated by AFD. While the introduction of $b > 0$ results in a slight increase in FID and NFE, we believe this trade-off is advantageous in certain scenarios.

Model	Sampler	NFEs \downarrow	FID \downarrow	AFD \uparrow
DDBM-VP	DDBM	118	1.83	6.99
DDBM-VP	SDB	40	1.16	6.29
Linear ($b = 0$)	SDB	5	0.89	6.00
Linear ($b = 0.5$)	SDB	40	1.71	9.52

that by introducing booting noise to the input data distribution, the model can generate samples with more diverse colors and textures. Further quantitative results are presented in Table 4, confirming that our model surpasses the vanilla DDBM in terms of image quality, sample efficiency, and conditional diversity.

6 Related Work

Diffusion Bridge Models. Diffusion bridges are faster diffusion processes that could learn the mapping between two random target distributions (Yifeng Shi et al., 2023; Stefano Peluchetti, 2023), demonstrating significant potential in various areas, such as protein docking (Somnath et al., 2023), mean-field game (Liu et al., 2022a), I2I translation (Liu et al., 2023; Linqi Zhou et al., 2023). According to different design philosophies, DBMs can be divided into two groups: bridge matching and stochastic interpolants. The idea of bridge matching was first proposed by Peluchetti (2023), and can be viewed as a generalization of score matching (Song et al., 2020). Based on this, diffusion Schrödinger bridge matching (DSBM) has been developed for solving Schrödinger bridge problems Stefano Peluchetti (2023); Yifeng Shi et al. (2023). In addition, Liu et al. (2023) utilize bridge matching to perform image restoration tasks and noted benefits of stochasticity empirically, the experiments shows the new model is more efficient and interpretable than score-based generative models (Liu et al., 2023). Furthermore, our benchmark DDBM (Linqi Zhou et al., 2023) achieve significant improvement for various I2I translation tasks. Flow Matching and Rectified Flow learn ODE models to facilitate transport between two empirically observed distributions (Lipman et al., 2022; Liu et al., 2022b). Stochastic interpolants further couple the base and target densities through SDEs (Albergo et al., 2023). Although our approach aligns with these methods, it diverges in various aspects. Unlike stochastic interpolation which models the data distribution p_0 , our framework specifically targets sampling from the conditional distribution $p_{0|T}$, significantly simplifying both training and inference. Furthermore, our approach is the first to highlight the importance of introducing stochasticity into the base distribution.

Image-to-Image Translations. Diffusion models have shown extraordinary performance in image synthesis. However, enhancing their capability in I2I translation presents several challenges, primarily the reduction of artifacts in translated images. To address this, DiffI2I mitigates misalignment and reduces artifacts in I2I translation tasks with fewer diffusion steps (Bin Xia et al., 2023). In the latent space, I2I translation is also achieved more quickly by S2ST (Or Greenberg et al., 2023), which consumes less memory. Various methods leverage different forms of guidance (Narek Tumanyan et al., 2023; Hyunsoo Lee et al., 2023), such as frequency control (Xiang Gao et al., 2024), to tackle these challenges. Another significant challenge is that I2I translation methods typically require joint training on both

source and target domains, posing privacy concerns. Injecting-diffusion addresses this issue in unpaired I2I translation by extracting domain-independent content from the source image and fusing it into the target domain (Luying Li & Lizhuang Ma, 2023). To improve interpretability in unpaired translation, SDMM separates intermediate tangled generative distributions by decomposing the score function (Shurong Sun et al., 2023). Diffusion bridges are also popular due to their interpretability and ability to map between arbitrary distributions. DDIB employs an encoder trained on the source domain and a decoder trained on the target domain to establish Schrödinger Bridges (SBs) (Xu Su et al., 2022). Beomsu Kim et al. (2023) incorporates discriminators and regularization to learn an SB between unpaired data.

7 Conclusion

In this study, we introduced the Stochasticity-controlled Diffusion Bridge (SDB), a framework designed to facilitate translation between two arbitrary distributions. By strategically managing stochasticity in the base distribution, transition kernel, and sampling SDEs, our approach improves image quality, sampling efficiency, and conditional diversity, allowing for the tailored design of diffusion bridge models across a range of tasks. We highlighted the importance of stochasticity control (SC) and addressed challenges associated with singularity through score reparameterization and specially designed discretization. Our results demonstrate that a simple linear bridge configuration can set new benchmarks in image quality, sampling efficiency and conditional diversity, as evidenced by our experiments with 64×64 edges2handbags and 256×256 DIODE-outdoor I2I translation tasks. Despite these advancements, we acknowledge that the optimal control of stochasticity may vary from one scenario to another, indicating a rich avenue for further exploration and refinement in future work.

References

Michael S Albergo, Nicholas M Boffi, and Eric Vanden-Eijnden. Stochastic interpolants: A unifying framework for flows and diffusions. *arXiv preprint arXiv:2303.08797*, 2023.

Shane Barratt and Rishi Sharma. A note on the inception score. *arXiv preprint arXiv:1801.01973*, 2018.

Beomsu Kim, Gihyun Kwon, Kwanyoung Kim, and Jong Chul Ye. Unpaired Image-to-Image Translation via Neural Schrödinger Bridge. *arXiv.org*, 2023. doi: 10.48550/arxiv.2305.15086.

Bin Xia, Yulun Zhang, Shiyin Wang, Yitong Wang, Xiaohong Wu, Yapeng Tian, Wenge Yang, Radu Timofte, and Luc Van Gool. DiffI2I: Efficient Diffusion Model for Image-to-Image Translation. *arXiv.org*, 2023. doi: 10.48550/arxiv.2308.13767.

Prafulla Dhariwal and Alexander Nichol. Diffusion models beat gans on image synthesis. *Advances in neural information processing systems*, 34:8780–8794, 2021.

Martin Heusel, Hubert Ramsauer, Thomas Unterthiner, Bernhard Nessler, and Sepp Hochreiter. Gans trained by a two time-scale update rule converge to a local nash equilibrium. *Advances in neural information processing systems*, 30, 2017.

Jonathan Ho, Ajay Jain, and Pieter Abbeel. Denoising diffusion probabilistic models. *Advances in neural information processing systems*, 33:6840–6851, 2020.

Hyunsoo Lee, Minsoo Kang, and Bohyung Han. Conditional Score Guidance for Text-Driven Image-to-Image Translation. *Neural Information Processing Systems*, 2023. doi: 10.48550/arxiv.2305.18007.

Phillip Isola, Jun-Yan Zhu, Tinghui Zhou, and Alexei A Efros. Image-to-image translation with conditional adversarial networks. In *Proceedings of the IEEE conference on computer vision and pattern recognition*, pp. 1125–1134, 2017.

Tero Karras, Miika Aittala, Timo Aila, and Samuli Laine. Elucidating the design space of diffusion-based generative models. *Advances in neural information processing systems*, 35:26565–26577, 2022.

Linqi Zhou, Aaron Lou, Samar Khanna, and Stefano Ermon. Denoising Diffusion Bridge Models. *arXiv.org*, 2023. doi: 10.48550/arxiv.2309.16948.

Yaron Lipman, Ricky TQ Chen, Heli Ben-Hamu, Maximilian Nickel, and Matt Le. Flow matching for generative modeling. *arXiv preprint arXiv:2210.02747*, 2022.

Guan-Horng Liu, Tianrong Chen, Oswin So, and Evangelos Theodorou. Deep generalized schrödinger bridge. *Advances in Neural Information Processing Systems*, 35:9374–9388, 2022a.

Guan-Horng Liu, Arash Vahdat, De-An Huang, Evangelos A Theodorou, Weili Nie, and Anima Anandkumar. I²sb: Image-to-image schrödinger bridge. *arXiv preprint arXiv:2302.05872*, 2023.

Xingchao Liu, Chengyue Gong, and Qiang Liu. Flow straight and fast: Learning to generate and transfer data with rectified flow. *arXiv preprint arXiv:2209.03003*, 2022b.

Luying Li and Lizhuang Ma. Injecting-Diffusion: Inject Domain-Independent Contents into Diffusion Models for Unpaired Image-to-Image Translation. *IEEE International Conference on Multimedia and Expo*, 2023. doi: 10.1109/icme55011.2023.00056.

Chenlin Meng, Yutong He, Yang Song, Jiaming Song, Jiajun Wu, Jun-Yan Zhu, and Stefano Ermon. Sdedit: Guided image synthesis and editing with stochastic differential equations. *arXiv preprint arXiv:2108.01073*, 2021.

Narek Tumanyan, Michal Geyer, Shai Bagon, and Tali Dekel. Plug-and-Play Diffusion Features for Text-Driven Image-to-Image Translation. *Computer Vision and Pattern Recognition*, 2023. doi: 10.1109/cvpr52729.2023.00191.

Or Greenberg, Eran Kishon, and Dani Lischinski. S2ST: Image-to-Image Translation in the Seed Space of Latent Diffusion. *arXiv.org*, 2023. doi: 10.48550/arxiv.2312.00116.

Stefano Peluchetti. Non-denoising forward-time diffusions. *arXiv preprint arXiv:2312.14589*, 2023.

L Chris G Rogers and David Williams. *Diffusions, Markov processes, and martingales: Itô calculus*, volume 2. Cambridge university press, 2000.

Shurong Sun, Longhui Wei, Junliang Xing, Jia Jia, and Qi Tian. SDDM: Score-Decomposed Diffusion Models on Manifolds for Unpaired Image-to-Image Translation. *International Conference on Machine Learning*, 2023. doi: 10.48550/arxiv.2308.02154.

Vignesh Ram Somnath, Matteo Pariset, Ya-Ping Hsieh, Maria Rodriguez Martinez, Andreas Krause, and Charlotte Bunne. Aligned diffusion schrödinger bridges. In *Uncertainty in Artificial Intelligence*, pp. 1985–1995. PMLR, 2023.

Yang Song and Stefano Ermon. Generative modeling by estimating gradients of the data distribution. *Advances in neural information processing systems*, 32, 2019.

Yang Song, Jascha Sohl-Dickstein, Diederik P Kingma, Abhishek Kumar, Stefano Ermon, and Ben Poole. Score-based generative modeling through stochastic differential equations. *arXiv preprint arXiv:2011.13456*, 2020.

Stefano Peluchetti. Diffusion Bridge Mixture Transports, Schrödinger Bridge Problems and Generative Modeling. *arXiv.org*, 2023. doi: 10.48550/arxiv.2304.00917.

Xuan Su, Jiaming Song, Chenlin Meng, and Stefano Ermon. Dual diffusion implicit bridges for image-to-image translation. *arXiv preprint arXiv:2203.08382*, 2022.

Igor Vasiljevic, Nick Kolkin, Shanyi Zhang, Ruotian Luo, Haochen Wang, Falcon Z Dai, Andrea F Daniele, Mohammadreza Mostajabi, Steven Basart, Matthew R Walter, et al. Diode: A dense indoor and outdoor depth dataset. *arXiv preprint arXiv:1908.00463*, 2019.

Xiang Gao, Zhengbo Xu, Junhan Zhao, and Jiaying Liu. Frequency-Controlled Diffusion Model for Versatile Text-Guided Image-to-Image Translation. *AAAI Conference on Artificial Intelligence*, 2024. doi: 10.1609/aaai.v38i3.27951.

Xu Su, Jiaming Song, Chenlin Meng, and Stefano Ermon. Dual Diffusion Implicit Bridges for Image-to-Image Translation. *International Conference on Learning Representations*, 2022. doi: 10.48550/arxiv.2203.08382.

Yifeng Shi, Valentin De Bortoli, Andrew T. Campbell, and Arnaud Doucet. Diffusion Schrödinger Bridge Matching. *Neural Information Processing Systems*, 2023. doi: 10.48550/arxiv.2303.16852.

Richard Zhang, Phillip Isola, Alexei A Efros, Eli Shechtman, and Oliver Wang. The unreasonable effectiveness of deep features as a perceptual metric. In *Proceedings of the IEEE conference on computer vision and pattern recognition*, pp. 586–595, 2018.

Kaiwen Zheng, Guande He, Jianfei Chen, Fan Bao, and Jun Zhu. Diffusion bridge implicit models. *arXiv preprint arXiv:2405.15885*, 2024.

A Proofs

Lemma 1. *There exist a linear Itô SDE*

$$d\mathbf{X}_t = [f_t \mathbf{X}_t + s_t \mathbf{x}_T] dt + g_t d\mathbf{W}_t, \quad \mathbf{X}_0 = \mathbf{x}_0, \quad (21)$$

where $f_t = \frac{\dot{\alpha}_t}{\alpha_t}$, $s_t = \dot{\beta}_t - \frac{\dot{\alpha}_t}{\alpha_t} \beta_t$, $g_t = \sqrt{2(\gamma_t \dot{\gamma}_t - \frac{\dot{\alpha}_t}{\alpha_t} \gamma_t^2)}$, that has a Gaussian marginal distribution $\mathcal{N}(\mathbf{x}_t; \alpha_t \mathbf{x}_0 + \beta_t \mathbf{x}_T, \gamma_t^2 \mathbf{I})$.

Proof. Let \mathbf{m}_t denote the mean function of the given Itô SDE, then we have $\frac{d\mathbf{m}_t}{dt} = f_t \mathbf{m}_t + s_t \mathbf{x}_T$. Given the transition kernel, the mean function $\mathbf{m}_t = \alpha_t \mathbf{x}_0 + \beta_t \mathbf{x}_T$, therefore,

$$\dot{\alpha}_t \mathbf{x}_0 + \dot{\beta}_t \mathbf{x}_T = f_t(\alpha_t \mathbf{x}_0 + \beta_t \mathbf{x}_T) + s_t \mathbf{x}_T. \quad (22)$$

Matching the above equation:

$$f_t = \frac{\dot{\alpha}_t}{\alpha_t}, \quad s_t = \dot{\beta}_t - \beta_t \frac{\dot{\alpha}_t}{\alpha_t}. \quad (23)$$

Further, For the variance γ_t^2 of the process, the dynamics are given by:

$$\frac{d\gamma_t^2}{dt} = 2f_t \gamma_t^2 + g_t^2. \quad (24)$$

Solving for g_t^2 , we substitute $f_t = \frac{\dot{\alpha}_t}{\alpha_t}$:

$$g_t^2 = \frac{d\gamma_t^2}{dt} - 2 \frac{\dot{\alpha}_t}{\alpha_t} \gamma_t^2 \quad (25)$$

Therefore,

$$g_t = \sqrt{2(\gamma_t \dot{\gamma}_t - \frac{\dot{\alpha}_t}{\alpha_t} \gamma_t^2)}. \quad (26)$$

□

Lemma 2. *Consider a continuous dynamics given by ODE of the form: $d\mathbf{X}_t = \mathbf{u}_t dt$, with the density evolution $p_t(\mathbf{X}_t)$. Then there exists forward SDEs and backward SDEs that match the marginal distribution p_t . The forward SDEs are given by: $d\mathbf{X}_t = (\mathbf{u}_t + \epsilon_t \nabla \log p_t) dt + \sqrt{2\epsilon_t} d\mathbf{W}_t$, $\epsilon_t > 0$. The backward SDEs are given by: $d\mathbf{X}_t = (\mathbf{u}_t - \epsilon_t \nabla \log p_t) dt + \sqrt{2\epsilon_t} d\mathbf{W}_t$, $\epsilon_t > 0$.*

Proof. For the forward SDEs, the Fokker-Planck equations are given by:

$$\frac{\partial p_t(\mathbf{X}_t)}{\partial t} = -\nabla \cdot [(\mathbf{u}_t + \epsilon_t \nabla \log p_t) p_t(\mathbf{X}_t)] + \epsilon_t \nabla^2 p_t(\mathbf{X}_t) \quad (27)$$

$$= -\nabla \cdot [\mathbf{u}_t p_t(\mathbf{X}_t)] - \nabla \cdot [\epsilon_t (\nabla \log p_t) p_t(\mathbf{X}_t)] + \epsilon_t \nabla^2 p_t(\mathbf{X}_t) \quad (28)$$

$$= -\nabla \cdot [\mathbf{u}_t p_t(\mathbf{X}_t)] - \epsilon_t \nabla \cdot [\nabla p_t(\mathbf{X}_t)] + \epsilon_t \nabla^2 p_t(\mathbf{X}_t) \quad (29)$$

$$= -\nabla \cdot [\mathbf{u}_t p_t(\mathbf{X}_t)]. \quad (30)$$

This is exactly the Fokker-Planck equation for the original deterministic ODE $d\mathbf{X}_t = \mathbf{u}_t dt$. Therefore, the forward SDE maintains the same marginal distribution $p_t(\mathbf{X}_t)$ as the original ODE.

Now consider the backward SDEs, the Fokker-Planck equations become:

$$\frac{\partial p_t(\mathbf{X}_t)}{\partial t} = -\nabla \cdot [(\mathbf{u}_t - \epsilon_t \nabla \log p_t) p_t(\mathbf{X}_t)] - \epsilon_t \nabla^2 p_t(\mathbf{X}_t) \quad (31)$$

$$= -\nabla \cdot [\mathbf{u}_t p_t(\mathbf{X}_t)] + \nabla \cdot [\epsilon_t (\nabla \log p_t) p_t(\mathbf{X}_t)] - \epsilon_t \nabla^2 p_t(\mathbf{X}_t) \quad (32)$$

$$= -\nabla \cdot [\mathbf{u}_t p_t(\mathbf{X}_t)]. \quad (33)$$

This is again the Fokker-Planck equation corresponding to the original deterministic ODE $d\mathbf{X}_t = \mathbf{u}_t dt$. Therefore, the backward SDE also maintains the same marginal distribution $p_t(\mathbf{X}_t)$. \square

Theorem 3. Suppose the transition kernel of a diffusion process is given by $p_{t|0,T}(\mathbf{x}_t \mid \mathbf{x}_0, \mathbf{x}_T) = \mathcal{N}(\mathbf{x}_t; \alpha_t \mathbf{x}_0 + \beta_t \mathbf{x}_T, \gamma_t^2 \mathbf{I})$, then the evolution of conditional probability $q(\mathbf{X}_t \mid \mathbf{x}_T)$ has a class of time reverse sampling SDEs of the form:

$$d\mathbf{X}_t = \left[\dot{\alpha}_t \hat{\mathbf{x}}_0 + \dot{\beta}_t \mathbf{x}_T - (\dot{\gamma}_t \gamma_t + \epsilon_t) \nabla_{\mathbf{X}_t} \log p_t(\mathbf{X}_t \mid \mathbf{x}_T) \right] dt + \sqrt{2\epsilon_t} d\mathbf{W}_t \quad \mathbf{X}_T = \mathbf{x}_T. \quad (34)$$

Proof. Recall Eqs. (10) 11 and Lemma 2,

$$d\mathbf{X}_t = \left[\frac{\dot{\alpha}_t}{\alpha_t} \mathbf{x}_t + \left(\dot{\beta}_t - \frac{\dot{\alpha}_t}{\alpha_t} \beta_t \right) \mathbf{x}_T - \left(\gamma_t \dot{\gamma}_t - \frac{\dot{\alpha}_t}{\alpha_t} \gamma_t^2 + \epsilon_t \right) \nabla_{\mathbf{x}_t} \log p_t(\mathbf{x}_t \mid \mathbf{x}_T) \right] dt + \sqrt{2\epsilon_t} d\mathbf{w}_t. \quad (35)$$

\square

Next we take the reparameterized score 15 into 35:

$$d\mathbf{X}_t = \left[\frac{\dot{\alpha}_t}{\alpha_t} \mathbf{X}_t + \left(\dot{\beta}_t - \frac{\dot{\alpha}_t}{\alpha_t} \beta_t \right) \mathbf{x}_T - \left(\gamma_t \dot{\gamma}_t - \frac{\dot{\alpha}_t}{\alpha_t} \gamma_t^2 + \epsilon_t \right) \frac{\alpha_t \hat{\mathbf{x}}_0 + \beta_t \mathbf{x}_T - \mathbf{X}_t}{\gamma_t^2} \right] dt + \sqrt{2\epsilon_t} d\mathbf{w}_t \quad (36)$$

$$= \left[\dot{\alpha}_t \hat{\mathbf{x}}_0 + \dot{\beta}_t \mathbf{x}_T - \left(\gamma_t \dot{\gamma}_t + \epsilon_t \right) \frac{\alpha_t \hat{\mathbf{x}}_0 + \beta_t \mathbf{x}_T - \mathbf{X}_t}{\gamma_t^2} \right] dt + \sqrt{2\epsilon_t} d\mathbf{w}_t \quad (37)$$

$$= \left[\dot{\alpha}_t \hat{\mathbf{x}}_0 + \dot{\beta}_t \mathbf{x}_T - \left(\dot{\gamma}_t + \frac{\epsilon_t}{\gamma_t} \right) \frac{\alpha_t \hat{\mathbf{x}}_0 + \beta_t \mathbf{x}_T - \mathbf{X}_t}{\gamma_t} \right] dt + \sqrt{2\epsilon_t} d\mathbf{w}_t \quad (38)$$

$$= \left[\dot{\alpha}_t \hat{\mathbf{x}}_0 + \dot{\beta}_t \mathbf{x}_T - \left(\dot{\gamma}_t + \frac{\epsilon_t}{\gamma_t} \right) \hat{\mathbf{z}} \right] dt + \sqrt{2\epsilon_t} d\mathbf{w}_t. \quad (39)$$

Theorem 4. Let $(\mathbf{x}_0, \mathbf{x}_T) \sim \pi_0(\mathbf{x}_0, \mathbf{x}_T)$, $\mathbf{x}_t \sim p_t(\mathbf{x} \mid \mathbf{x}_0, \mathbf{x}_T)$, Given the transition kernel: $p(\mathbf{x}_t \mid \mathbf{x}_0, \mathbf{x}_T) = \mathcal{N}(\mathbf{x}_t; \alpha_t \mathbf{x}_0 + \beta_t \mathbf{x}_T, \gamma_t^2 \mathbf{I})$, if $\hat{\mathbf{x}}_0(\mathbf{x}_t, \mathbf{x}_T, t)$ is a denoiser function that minimizes the expected L_2 denoising error for samples drawn from $\pi_0(\mathbf{x}_0, \mathbf{x}_T)$:

$$\hat{\mathbf{x}}_0(\mathbf{x}_t, \mathbf{x}_T, t) = \arg \min_{D(\mathbf{x}_t, \mathbf{x}_T, t)} \mathbb{E}_{\mathbf{x}_0, \mathbf{x}_T, \mathbf{x}_t} [\lambda(t) \|D(\mathbf{x}_t, \mathbf{x}_T, t) - \mathbf{x}_0\|_2^2], \quad (40)$$

then the score has the following relationship with $\hat{\mathbf{x}}_0(\mathbf{x}_t, \mathbf{x}_T, t)$:

$$\nabla_{\mathbf{x}_t} \log p_t(\mathbf{x}_t \mid \mathbf{x}_T) = \frac{\alpha_t \hat{\mathbf{x}}_0(\mathbf{x}_t, \mathbf{x}_T, t) + \beta_t \mathbf{x}_T - \mathbf{x}_t}{\gamma_t^2}. \quad (41)$$

Proof.

$$\mathcal{L}(D) = \mathbb{E}_{(\mathbf{x}_0, \mathbf{x}_T) \sim \pi_0(\mathbf{x}_0, \mathbf{x}_T)} \mathbb{E}_{\mathbf{x}_t \sim p_t(\mathbf{x}_t \mid \mathbf{x}_0, \mathbf{x}_T)} \|D(\mathbf{x}_t) - \mathbf{x}_0\|_2^2 \quad (42)$$

$$= \int_{\mathbb{R}^d} \int_{\mathbb{R}^d} \underbrace{\int_{\mathbb{R}^d} p_t(\mathbf{x}_t \mid \mathbf{x}_0, \mathbf{x}_T) \pi_0(\mathbf{x}_0, \mathbf{x}_T) \|D(\mathbf{x}_t) - \mathbf{x}_0\|_2^2 d\mathbf{x}_0 d\mathbf{x}_T d\mathbf{x}_t}_{=: \mathcal{L}(D; \mathbf{x}_t, \mathbf{x}_T)}, \quad (43)$$

$$\mathcal{L}(D; \mathbf{x}_t, \mathbf{x}_T) = \int_{\mathbb{R}^d} p_t(\mathbf{x}_t | \mathbf{x}_0, \mathbf{x}_T) \pi_0(\mathbf{x}_0, \mathbf{x}_T) \|D(\mathbf{x}_t) - \mathbf{x}_0\|_2^2 d\mathbf{x}_0, \quad (44)$$

we can minimize $\mathcal{L}(D)$ by minimizing $\mathcal{L}(D; \mathbf{x}_t, \mathbf{x}_T)$ independently for each $\{\mathbf{x}_t, \mathbf{x}_T\}$ pair.

$$D^*(\mathbf{x}_t, \mathbf{x}_T) = \arg \min_{D(\mathbf{x}_t)} \mathcal{L}(D; \mathbf{x}_t, \mathbf{x}_T) \quad (45)$$

$$\mathbf{0} = \nabla_{D(\mathbf{x}_t, \mathbf{x}_T)} [\mathcal{L}(D; \mathbf{x}_t, \mathbf{x}_T)] \quad (46)$$

$$= \int_{\mathbb{R}^d} p_t(\mathbf{x}_t | \mathbf{x}_0, \mathbf{x}_T) \pi_0(\mathbf{x}_0, \mathbf{x}_T) 2[D(\mathbf{x}, \mathbf{x}_T) - \mathbf{x}_0] d\mathbf{x}_0 \quad (47)$$

$$= 2[D(\mathbf{x}_t, \mathbf{x}_T) \int_{\mathbb{R}^d} p_t(\mathbf{x}_t | \mathbf{x}_0, \mathbf{x}_T) \pi_0(\mathbf{x}_0, \mathbf{x}_T) d\mathbf{x}_0 - \int_{\mathbb{R}^d} p_t(\mathbf{x}_t | \mathbf{x}_0, \mathbf{x}_T) \pi_0(\mathbf{x}_0, \mathbf{x}_T) \mathbf{x}_0 d\mathbf{x}_0] \quad (48)$$

$$= 2[D(\mathbf{x}) p_t(\mathbf{x}_t, \mathbf{x}_T) - \int_{\mathbb{R}^d} p_t(\mathbf{x}_t | \mathbf{x}_0, \mathbf{x}_T) \pi_0(\mathbf{x}_0, \mathbf{x}_T) \mathbf{x}_0 d\mathbf{x}_0], \quad (49)$$

$$D^*(\mathbf{x}_t, \mathbf{x}_T) = \int_{\mathbb{R}^d} \frac{p_t(\mathbf{x}_t | \mathbf{x}_0, \mathbf{x}_T) \pi_0(\mathbf{x}_0, \mathbf{x}_T) \mathbf{x}_0}{p_t(\mathbf{x}_t, \mathbf{x}_T)} d\mathbf{x}_0, \quad (50)$$

$$\nabla_{\mathbf{x}_t} \log p_t(\mathbf{x}_t | \mathbf{x}_T) = \frac{\nabla_{\mathbf{x}_t} p_t(\mathbf{x}_t, \mathbf{x}_T)}{p_t(\mathbf{x}_t, \mathbf{x}_T)} \quad (51)$$

$$= \frac{\int \nabla_{\mathbf{x}_t} p_t(\mathbf{x}_t | \mathbf{x}_T, \mathbf{x}_0) \pi_0(\mathbf{x}_0, \mathbf{x}_T) d\mathbf{x}_0}{p_t(\mathbf{x}_t, \mathbf{x}_T)} \quad (52)$$

$$= - \int \frac{\mathbf{x}_t - \alpha_t \mathbf{x}_0 - \beta_t \mathbf{x}_T}{\gamma^2} \frac{p_t(\mathbf{x}_t | \mathbf{x}_0, \mathbf{x}_T) \pi_0(\mathbf{x}_0, \mathbf{x}_T)}{p_t(\mathbf{x}_t, \mathbf{x}_T)} d\mathbf{x}_0 \quad (53)$$

$$= \frac{\alpha_t D^*(\mathbf{x}_t, \mathbf{x}_T) + \beta_t \mathbf{x}_T - \mathbf{x}_t}{\gamma^2}. \quad (54)$$

Thus we conclude the proof. \square

B Reframing previous methods in our framework

We draw a link between our framework and the diffusion bridge models used in DDBM.

B.1 DDBM-VE

DDBM-VE can be reformulated in our framework as we set :

$$\alpha_t = s_t \left(1 - \frac{\sigma_t^2}{\sigma_T^2}\right), \beta_t = \frac{s_t \sigma_t^2}{s_1 \sigma_T^2}, \gamma_t = \sigma_t s_t \sqrt{\left(1 - \frac{\sigma_t^2}{\sigma_T^2}\right)} \quad (55)$$

Proof. In the origin DDBM paper, the evolution of conditional probability $q(\mathbf{x}_t | \mathbf{x}_T)$ has a time reversed SDE of the form:

$$d\mathbf{X}_t = [\bar{\mathbf{f}}_t(\mathbf{X}_t) - \bar{g}_t^2 \bar{\mathbf{h}}_t(\mathbf{X}_t) - \bar{g}_t^2 \mathbf{s}_t(\mathbf{X}_t)] dt + \bar{g}_t d\hat{\mathbf{W}}_t, \quad (56)$$

and an associated probability flow ODE

$$d\mathbf{X}_t = \left[\bar{\mathbf{f}}_t(\mathbf{X}_t) - \bar{g}_t^2 \bar{\mathbf{h}}_t(\mathbf{X}_t) - \frac{1}{2} \bar{g}_t^2 \mathbf{s}_t(\mathbf{X}_t) \right] dt. \quad (57)$$

Compare Eqs. (56) and 57 with Lemma 1. We only need to prove:

$$\bar{\mathbf{f}}_t(\mathbf{X}_t) - \bar{g}_t^2 \bar{\mathbf{h}}_t(\mathbf{X}_t) = f_t \mathbf{X}_t + s_t \mathbf{x}_T, \bar{g}_t = g_t. \quad (58)$$

In the original paper,

$$\bar{\mathbf{f}}_t(\mathbf{X}_t) = 0, \bar{g}_t^2 = \frac{d}{dt} \sigma_t^2, \bar{\mathbf{h}}_t(\mathbf{X}_t) = \frac{\mathbf{x}_T - \mathbf{x}_t}{\sigma_T^2 - \sigma_t^2}. \quad (59)$$

Therefore,

$$\bar{\mathbf{f}}_t(\mathbf{X}_t) - \bar{g}_t^2 \bar{\mathbf{h}}_t(\mathbf{X}_t) = \frac{2\sigma_t \dot{\sigma}_t (\mathbf{x}_T - \mathbf{x}_t)}{\sigma_T^2 - \sigma_t^2}, \bar{g}_t^2 = 2\dot{\sigma}_t \sigma_t. \quad (60)$$

In our framework, f_t, s_t, g_t^2 can be calculated:

$$f_t = \frac{\dot{\alpha}_t}{\alpha_t} = \frac{d}{dt} \log \alpha_t = \frac{d}{dt} \log \frac{\sigma_T^2 - \sigma_t^2}{\sigma_T^2} = \frac{-2\sigma_t \dot{\sigma}_t}{\sigma_T^2 - \sigma_t^2}, \quad (61)$$

$$s_t = \dot{\beta}_t - \frac{\dot{\alpha}_t}{\alpha_t} \beta_t = \frac{2\sigma_t \dot{\sigma}_t}{\sigma_T^2} + \frac{2\sigma_t \dot{\sigma}_t}{\sigma_T^2 - \sigma_t^2} \cdot \frac{\sigma_t^2}{\sigma_T^2} = \frac{2\sigma_t \dot{\sigma}_t}{\sigma_T^2 - \sigma_t^2}. \quad (62)$$

$$g_t^2 = 2(\gamma_t \dot{\gamma}_t - \frac{\dot{\alpha}_t}{\alpha_t} \gamma_t^2) = 2\gamma_t^2 \left(\frac{\dot{\gamma}_t}{\gamma_t} - \frac{\dot{\alpha}_t}{\alpha_t} \right) = \gamma_t^2 \left(\frac{(\sigma_T^2 - 2\sigma_t^2) \dot{\sigma}_t}{(\sigma_T^2 - \sigma_t^2) \sigma_t} + \frac{2\dot{\sigma}_t \sigma_t}{\sigma_T^2 - \sigma_t^2} \right) = 2\sigma_t \dot{\sigma}_t. \quad (63)$$

Therefore,

$$f_t \mathbf{X}_t + s_t \mathbf{x}_T = \frac{2\sigma_t \dot{\sigma}_t (\mathbf{x}_T - \mathbf{x}_t)}{\sigma_T^2 - \sigma_t^2} = \bar{\mathbf{f}}_t(\mathbf{X}_t) - \bar{g}_t^2 \bar{\mathbf{h}}_t(\mathbf{X}_t), \quad \bar{g}_t = g_t, \quad (64)$$

which matches the formulation in DDBM.

□

B.2 DDBM-VP

DDBM-VP can be reformulated in our framework as we set :

$$\alpha_t = a_t \left(1 - \frac{\sigma_t^2 a_1^2}{\sigma_1^2 a_t^2} \right), \beta_t = \frac{\sigma_t^2 a_1}{\sigma_1^2 a_t}, \gamma_t = \sqrt{\sigma_t^2 \left(1 - \frac{\sigma_t^2 a_1^2}{\sigma_1^2 a_t^2} \right)}. \quad (65)$$

Proof. In the original DDBM-VP setting,

$$\bar{\mathbf{f}}_t(\mathbf{X}_t) = \frac{d \log a_t}{dt} \mathbf{x}_t, \quad (66)$$

$$\bar{g}_t^2 = 2\sigma_t \dot{\sigma}_t - 2 \frac{\dot{a}_t}{a_t} \sigma_t^2 = \frac{2\sigma_t \dot{\sigma}_t a_t - 2\sigma_t^2 \dot{a}_t}{a_t}, \quad (67)$$

$$\bar{\mathbf{h}}_t(\mathbf{X}_t) = \frac{(a_t/a_1) \mathbf{x}_T - \mathbf{x}_t}{\sigma_t^2 (\text{SNR}_t/\text{SNR}_1 - 1)} = \frac{a_1 a_t \mathbf{x}_T - a_1^2 \mathbf{x}_t}{\sigma_1^2 a_t^2 - \sigma_t^2 a_1^2}. \quad (68)$$

Therefore,

$$\bar{\mathbf{f}}_t(\mathbf{X}_t) - \bar{g}_t^2 \bar{\mathbf{h}}_t(\mathbf{X}_t) = \left[\frac{\dot{a}_t}{a_t} - \frac{2\sigma_t a_1^2 (\dot{\sigma}_t a_t - \sigma_t \dot{a}_t)}{a_t (\sigma_1^2 a_t^2 - \sigma_t^2 a_1^2)} \right] \mathbf{x}_t + \frac{2\sigma_t a_1 (\dot{\sigma}_t a_t - \sigma_t \dot{a}_t)}{\sigma_1^2 a_t^2 - \sigma_t^2 a_1^2} \mathbf{x}_T. \quad (69)$$

In our framework, f_t, s_t, g_t^2 can be calculated:

$$f_t = \frac{\dot{\alpha}_t}{\alpha_t} = \frac{d}{dt} \log \alpha_t \quad (70)$$

$$= \frac{d}{dt} \log \frac{\sigma_1^2 a_t^2 - \sigma_t^2 a_1^2}{\sigma_1^2 a_t} \quad (71)$$

$$= \frac{2\sigma_1^2 a_t \dot{a}_t - 2a_1^2 \sigma_t \dot{\sigma}_t}{\sigma_1^2 a_t^2 - \sigma_t^2 a_1^2} - \frac{\dot{a}_t}{a_t} \quad (72)$$

$$= \frac{\dot{a}_t}{a_t} - \frac{2a_1^2 \sigma_t (a_t \dot{\sigma}_t - \dot{a}_t \sigma_t)}{a_t (\sigma_1^2 a_t^2 - \sigma_t^2 a_1^2)}, \quad (73)$$

$$s_t = \dot{\beta}_t - \frac{\dot{\alpha}_t}{\alpha_t} \beta_t = \beta_t \left(\frac{\dot{\beta}_t}{\beta_t} - \frac{\dot{\alpha}_t}{\alpha_t} \right) \quad (74)$$

$$= \frac{\sigma_t^2 a_1}{\sigma_1^2 a_t} \left(\frac{2\dot{\sigma}_t}{\sigma_t} - \frac{2\sigma_1^2 a_t \dot{a}_t - 2a_1^2 \sigma_t \dot{\sigma}_t}{\sigma_1^2 a_t^2 - \sigma_t^2 a_1^2} \right) \quad (75)$$

$$= \frac{2\sigma_t a_1 (\dot{\sigma}_t a_t - \sigma_t \dot{a}_t)}{\sigma_1^2 a_t^2 - \sigma_t^2 a_1^2}, \quad (76)$$

$$g_t^2 = \gamma_t \dot{\gamma}_t - \frac{\dot{\alpha}_t}{\alpha_t} \gamma_t^2 = \gamma_t^2 \left(\frac{\dot{\gamma}_t}{\gamma_t} - \frac{\dot{\alpha}_t}{\alpha_t} \right) \quad (77)$$

$$= \gamma^2 \frac{d}{dt} \log \frac{\gamma_t}{\alpha_t} \quad (78)$$

$$= \gamma^2 \frac{d}{dt} \left(\frac{1}{2} \log \frac{\sigma_t^2 \sigma_1^2}{\sigma_1^2 a_t^2 - \sigma_t^2 a_1^2} \right) \quad (79)$$

$$= \sigma_t^2 \left(1 - \frac{\sigma_t^2 a_1^2}{\sigma_1^2 a_t^2} \right) \left(\frac{\dot{\sigma}_t}{\sigma_t} - \frac{\sigma_1^2 a_t \dot{a}_t - a_1^2 \sigma_t \dot{\sigma}_t}{\sigma_1^2 a_t^2 - \sigma_t^2 a_1^2} \right) \quad (80)$$

$$= \frac{\dot{\sigma}_t \sigma_t a_t - \sigma_t^2 \dot{a}_t}{a_t}. \quad (81)$$

Therefore,

$$f_t \mathbf{X}_t + s_t \mathbf{x}_T = \bar{\mathbf{f}}_t(\mathbf{X}_t) - \bar{g}_t^2 \bar{\mathbf{h}}_t(\mathbf{X}_t), \bar{g}_t = g_t, \quad (82)$$

which matches the formulation in DDBM.

□

B.3 EDM

ODE formulation. The ODE formulation in EDM can be formulated in our framework as we set $\alpha_t = 1, \beta_t = 0, \gamma_t = \sigma_t$.

Proof. Recall 11, the ODE formulation is given by:

$$d\mathbf{X}_t = \left[f_t \mathbf{X}_t + s_t \mathbf{x}_T - \frac{1}{2} g_t^2 \nabla_{\mathbf{X}_t} \log p_t(\mathbf{X}_t | \mathbf{x}_T) \right] dt \quad \mathbf{X}_T = \mathbf{x}_T \quad (83)$$

where $f_t = \frac{\dot{\alpha}_t}{\alpha_t}, \quad s_t = \dot{\beta}_t - \frac{\dot{\alpha}_t}{\alpha_t} \beta_t, \quad g_t = \sqrt{2(\gamma_t \dot{\gamma}_t - \frac{\dot{\alpha}_t}{\alpha_t} \gamma_t^2)}$. As $\alpha_t = 1, \beta_t = 0, \gamma_t = \sigma_t$, The sampling ODE is given by:

$$d\mathbf{X}_t = -\sigma_t \dot{\sigma}_t \nabla_{\mathbf{X}_t} \log p_t(\mathbf{X}_t) dt \quad (84)$$

□

Denoising score matching. The score remarameterization in EDM is the same as ours in Eq. 15. Let $\alpha_t = 1, \beta_t = 0, \gamma_t = \sigma_t$, then the score reparameterization in Eq. 15 is given by:

$$\nabla_{\mathbf{x}_t} \log p_t(\mathbf{X}_t) \approx \frac{\hat{\mathbf{x}}_0 - \mathbf{x}_t}{\sigma_t^2}. \quad (85)$$

Sampling SDEs with stochasticity added. Recall Theorem 3, as $\alpha_t = 1, \beta_t = 0, \gamma_t = \sigma_t$, then the SDE has the form:

$$d\mathbf{X}_t = (-\sigma_t \dot{\sigma}_t + \epsilon_t) \nabla_{\mathbf{x}_t} \log p_t(\mathbf{X}_t) dt + \sqrt{2\epsilon_t} d\mathbf{W}_t. \quad (86)$$

Now we recover the stochastic sampling SDE in original EDM paper.

B.4 I2SB

I2SB can be reformulated in our framework as we let:

$$\alpha_t = 1 - \frac{\sigma_t^2}{\sigma_1^2}, \beta_t = \frac{\sigma_t^2}{\sigma_1^2}, \gamma_t = \sqrt{\sigma_t^2 \left(1 - \frac{\sigma_t^2}{\sigma_1^2}\right)} \quad (87)$$

where $\sigma_t^2 := \int_0^t \beta_\tau d\tau$.

Using discretization 20:

$$\mathbf{x}_{t-\Delta t} = (\alpha_{t-\Delta t} - \alpha_t \frac{\beta_{t-\Delta t}}{\beta_t}) \hat{\mathbf{x}}_0 + \frac{\beta_{t-\Delta t}}{\beta_t} \mathbf{x}_t + \sqrt{\gamma_{t-\Delta t}^2 - \frac{\beta_{t-\Delta t}^2 \gamma_t^2}{\beta_t^2}} \bar{\mathbf{z}}_t \quad (88)$$

$$= (1 - \frac{\beta_{t-\Delta t}}{\beta_t}) \hat{\mathbf{x}}_0 + \frac{\beta_{t-\Delta t}}{\beta_t} \mathbf{x}_t + \sqrt{\gamma_{t-\Delta t}^2 - \frac{\beta_{t-\Delta t}^2 \gamma_t^2}{\beta_t^2}} \bar{\mathbf{z}}_t \quad (89)$$

$$= (1 - \frac{\sigma_{t-\Delta t}^2}{\sigma_t^2}) \hat{\mathbf{x}}_0 + \frac{\sigma_{t-\Delta t}^2}{\sigma_t^2} \mathbf{x}_t + \sqrt{\frac{\sigma_{t-\Delta t}^2 \left(1 - \frac{\sigma_{t-\Delta t}^2}{\sigma_1^2}\right) \frac{\sigma_t^4}{\sigma_1^4} - \frac{\sigma_{t-\Delta t}^4}{\sigma_1^4} \sigma_t^2 \left(1 - \frac{\sigma_t^2}{\sigma_1^2}\right)}{\frac{\sigma_t^4}{\sigma_1^4}}} \bar{\mathbf{z}}_t \quad (90)$$

$$= (1 - \frac{\sigma_{t-\Delta t}^2}{\sigma_t^2}) \hat{\mathbf{x}}_0 + \frac{\sigma_{t-\Delta t}^2}{\sigma_t^2} \mathbf{x}_t + \sqrt{\frac{\sigma_{t-\Delta t}^2 (\sigma_t^2 - \sigma_{t-\Delta t}^2)}{\sigma_t^2}} \bar{\mathbf{z}}_t \quad (91)$$

In the I2SB paper, define $a_n^2 := \int_{t_n}^{t_{n+1}} \beta_\tau d\tau, \sigma_n^2 := \int_0^{t_n} \beta_\tau d\tau$. Therefore,

$$\mathbf{x}_n = \frac{a_n^2}{a_n^2 + \sigma_n^2} \hat{\mathbf{x}}_0 + \frac{\sigma_n^2}{a_n^2 + \sigma_n^2} \mathbf{x}_{n+1} + \sqrt{\frac{\sigma_n^2 a_n^2}{a_n^2 + \sigma_n^2}} \bar{\mathbf{z}}_t \quad (92)$$

Thus, we reproduce the sampler of I2SB.

C Experiment Details

Architecture. We maintain the architecture and parameter settings consistent with (Linqi Zhou et al., 2023), utilizing the ADM model (Dhariwal & Nichol, 2021) for 64×64 resolution, modifying the channel dimensions from 192 to 256 and reducing the number of residual blocks from three to two. Apart from these changes, all other settings remain identical to those used for 64×64 resolution.

Training. We include additional pre- and post-processing steps: scaling functions and loss weighting, the same ingredient as (Karras et al., 2022). Let $D_\theta(\mathbf{x}_t, \mathbf{x}_T, t) = c_{\text{skip}}(t)\mathbf{x}_t + c_{\text{out}(t)}(t)F_\theta(c_{\text{in}}(t)\mathbf{x}_t, c_{\text{noise}}(t))$, where F_θ is a neural network with parameter θ , the effective training target with respect to the raw network F_θ is:

$\mathbb{E}_{\mathbf{x}_t, \mathbf{x}_0, \mathbf{x}_T, t} [\lambda \|c_{\text{skip}}(\mathbf{x}_t + c_{\text{out}} F_\theta(c_{\text{in}} \mathbf{x}_t, c_{\text{noise}}) - \mathbf{x}_0\|^2]$. Scaling scheme are chosen by requiring network inputs and training targets to have unit variance ($c_{\text{in}}, c_{\text{out}}$), and amplifying errors in F_θ as little as possible. Following reasoning in (Linqi Zhou et al., 2023),

$$c_{\text{in}}(t) = \frac{1}{\sqrt{\alpha_t^2 \sigma_0^2 + \beta_t^2 \sigma_T^2 + 2\alpha_t \beta_t \sigma_{01} + \gamma_t^2}}, \quad c_{\text{skip}}(t) = (\alpha_t \sigma_0^2 + \beta_t \sigma_{01}) * c_{\text{in}}^2, \quad (93)$$

$$c_{\text{out}}(t) = \sqrt{\beta_t^2 \sigma_0^2 \sigma_1^2 - \beta_t^2 \sigma_{01}^2 + \gamma_t^2 \sigma_0^2} c_{\text{in}}, \quad \lambda = \frac{1}{c_{\text{out}}^2}, \quad c_{\text{noise}}(t) = \frac{1}{4} \log(t), \quad (94)$$

where σ_0^2, σ_T^2 , and σ_{0T} denote the variance of \mathbf{x}_0 , variance of \mathbf{x}_T and the covariance of the two, respectively.

We set $\sigma_0 = \sigma_T = 0.5, \sigma_{0T} = \sigma_0^2/2$ for all training sessions. Other setting are shown in Table 5.

Table 5: Training setting

Model	Dataset	edges→handbags	
		0	0.5
Setting	η	0.125	0.125
	γ_{max}	32	200
	GPU	1 A6000 48G	1 H100 96G
	Batch size	1×10^{-5}	1×10^{-4}
	Learning rate	9×10^6	1×10^6
	Iterations	42 days	11 days

Sampling. We use the same timesteps distributed according to EDM (Karras et al., 2022): $(t_{\text{max}}^{1/\rho} + \frac{i}{N}(t_{\text{min}}^{1/\rho} - t_{\text{max}}^{1/\rho}))^\rho$, where $t_{\text{min}} = 0.01$ and $t_{\text{max}} = 1 - 10^{-4}$. The best performance achieved by setting $\rho = 0.6$.

Licenses

- Edges→Handbags Isola et al. (2017): BSD license.
- DIODE-Outdoor Vasiljevic et al. (2019): MIT license.

D Additional visualizations

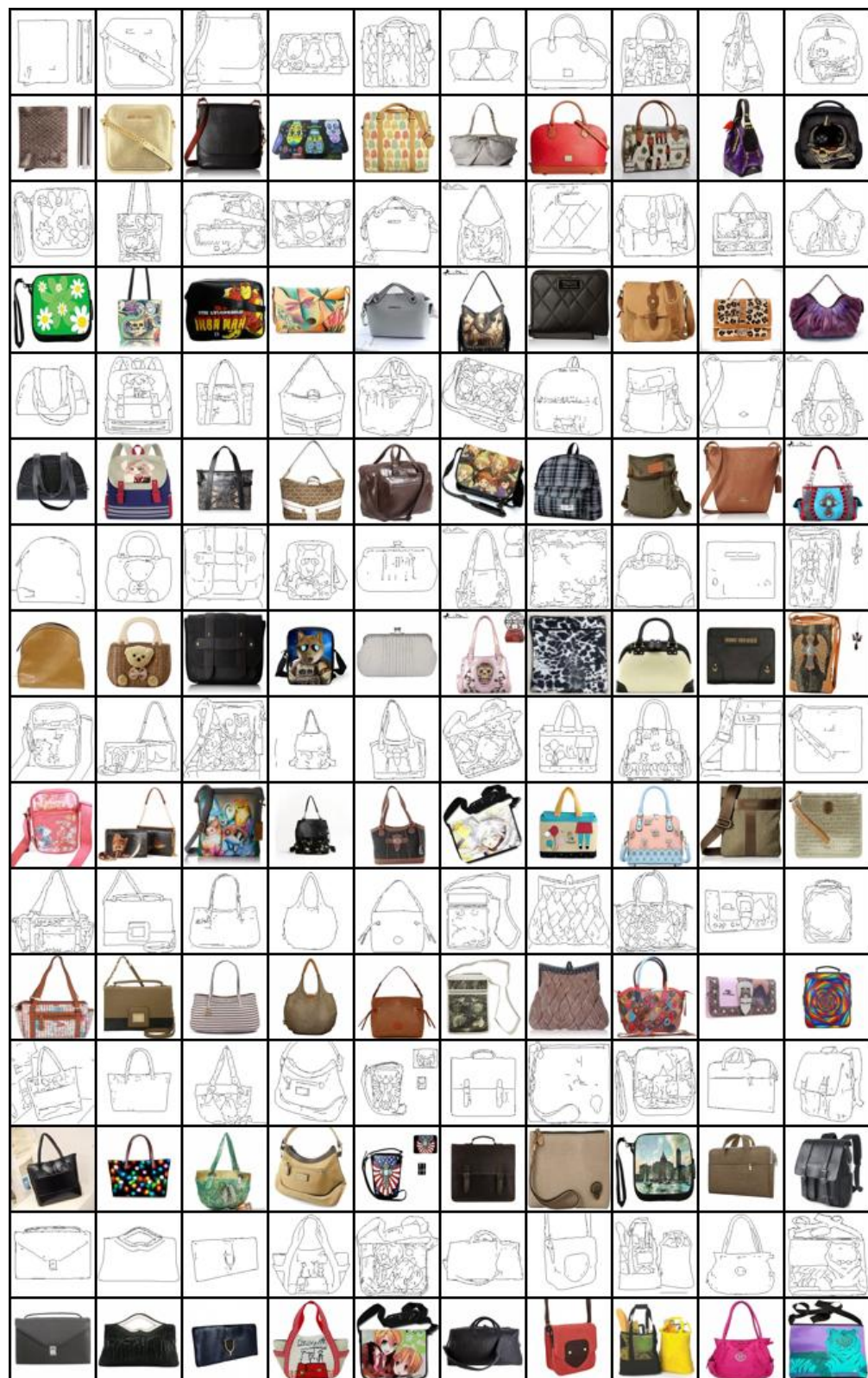


Figure 5: DDBM model and Our sampler (NFE=20, FID=1.53).

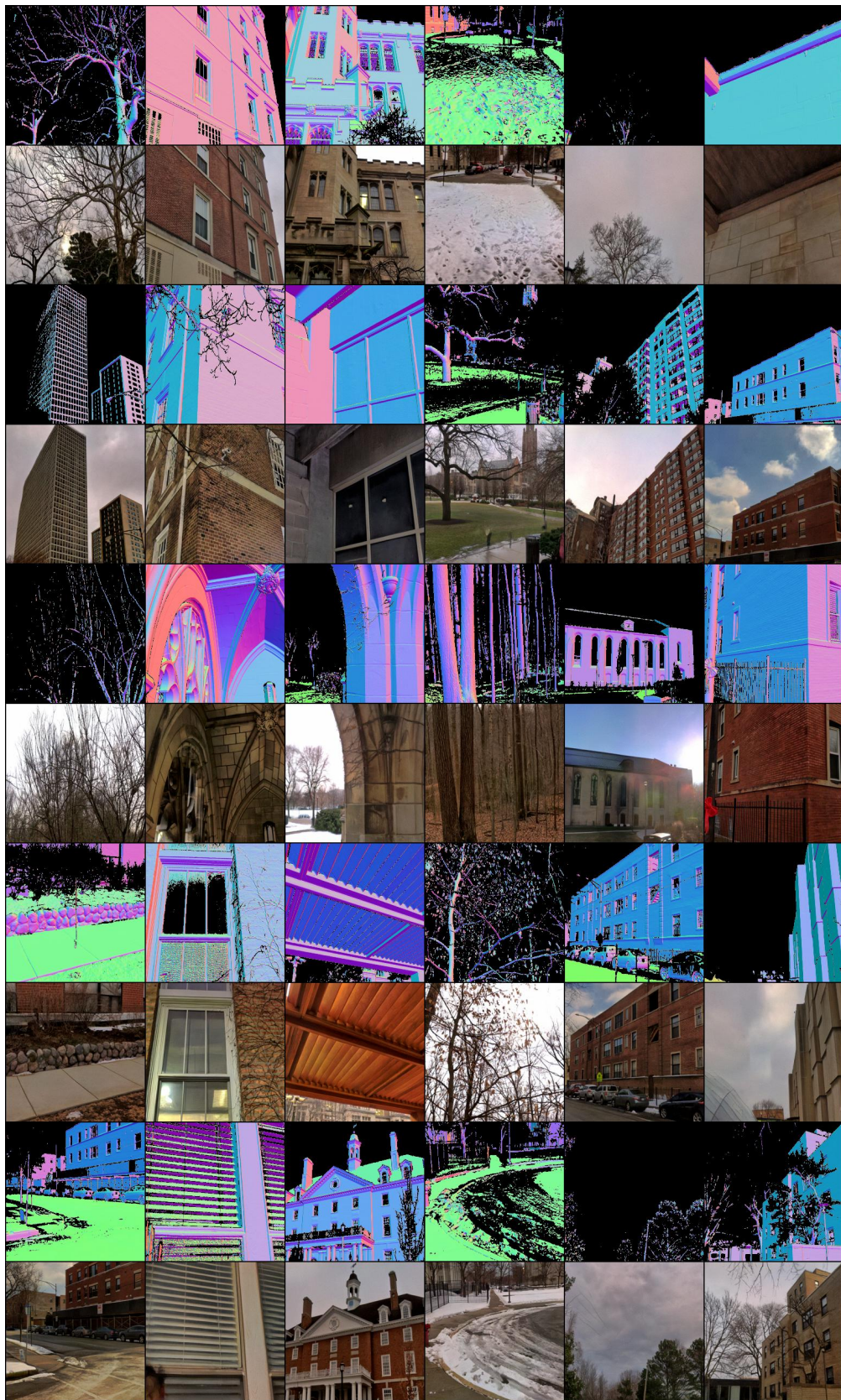


Figure 6: DDBM model and SDB sampler ($\eta = 0.3$, NFE=20, FID=4.12). Samples for DIODE dataset (conditioned on depth images).

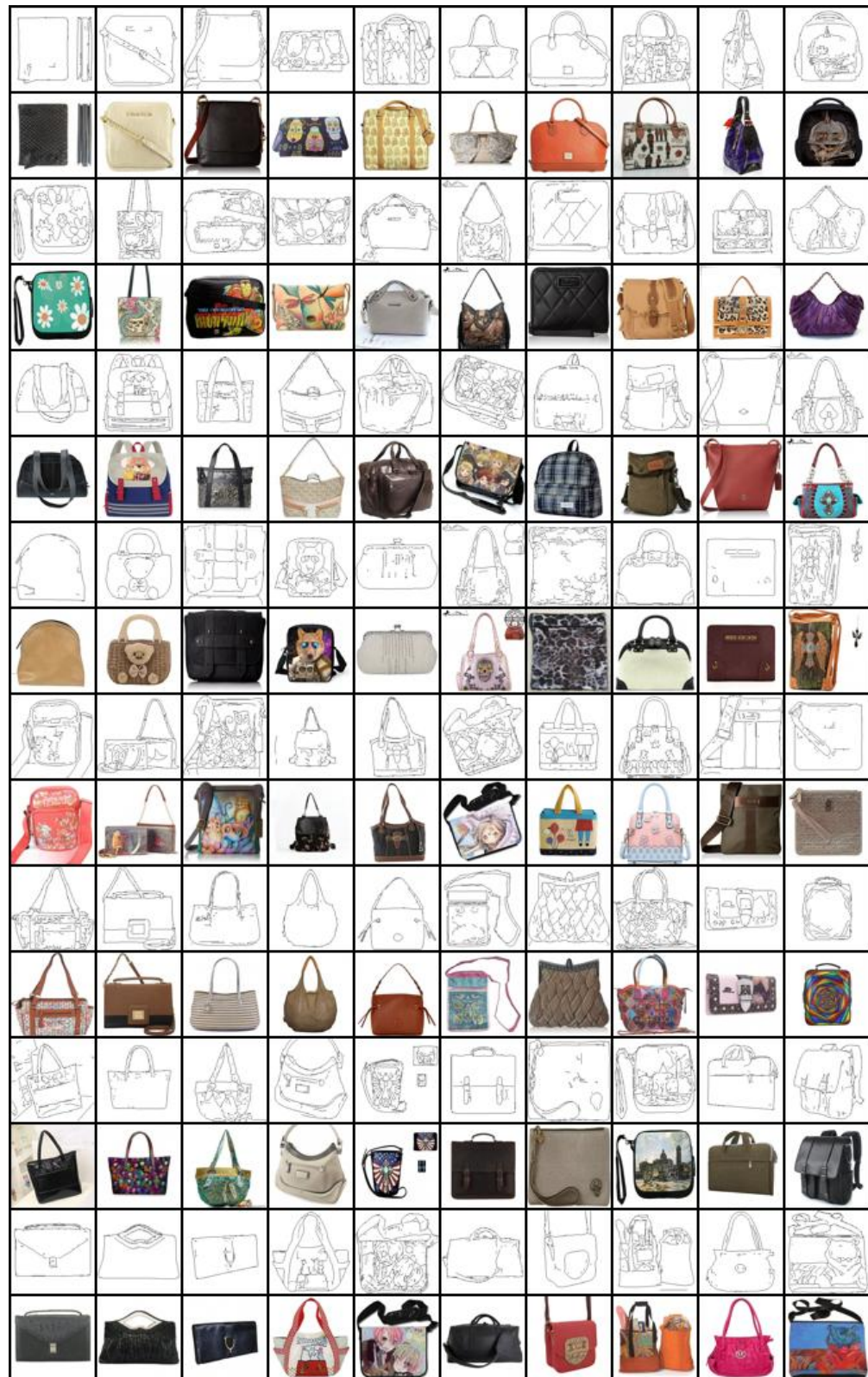
Figure 7: SDB model and sampler ($\gamma_{\max} = 0.125$, $\eta = 1$, $b = 0$, NFE=5, FID=0.89).



Figure 8: DDBM model and sampler (NFE=118, FID = 1.83, AFD=6.99).



Figure 9: SDB model and sampler ($\gamma_{\max} = 0.125$, $b = 0.5$, NFE=40, FID = 1.71, AFD=9.52).